Appendix 2

Definition of the matrix spalled lengths

A2.1   INTRODUCTION

The pullout response of an inclined steel fiber may be significantly influenced by the local interaction occurring at the point where the fiber exits the matrix. At this point, increasing deviation forces tend to produce spalling of small portions of the surrounding matrix. The estimation of the size of these portions is of great interest because it has a direct impact on the crack widths at which local frictional forces develop during the pullout process.

This appendix aims at providing a simplified procedure to quantify the length of matrix spalled off in the direction parallel to the original embedded axis of the fiber in terms of its inclination angle, the tensile strength of the concrete and the maximum axial load carried out by the fiber.

The first part of this appendix provides an approach to estimate the length of matrix spalled off on the pullout of inclined straight steel fibers (L_{SP1}) described in Chapter 4. Then, the increment of matrix spalled length induced by the hooked end (L_{SP2}) is calculated on the basis of a similar procedure. Once having both of these parameters the pullout model for hooked steel fibers described in Chapter 5 can be applied.

A2.2   DEFINITION OF L_{SP1}

Spalling of the matrix is a consequence of an extremely complex phenomenon in which failure of the matrix occurs due to local curvature and stretching of the fiber at the matrix cracked surface. However, depending upon a variety of parameters (fiber diameter and embedded length, fiber elastic modulus and tensile strength, magnitude and rate of external loading, etc.) the action imposed over the matrix wedge might change considerably. Moreover, regarding the magnitude of L_{SP1} in steel fiber reinforced cementitious matrices (up to few mm) uncertainties associated to the microstructure of the matrix might play a major effect.

To quantify the average matrix spalled length a simplified failure criterion is herein proposed taking into account the resisting mechanism provided by the matrix at the cracked surface (R_{SP1}) and the spalling force imposed by fiber curvature (F_{SP1}). Hence L_{SP1} represents the minimum length along fiber main axis at which the matrix wedge stabilizes, such as defined by Eq.A2.1.

$$R_{SP1} \geq F_{SP1} \tag{A2.1}$$

The resisting mechanism provided by the matrix (R_{SP1}) is based on the assumption that the tensile strength of the matrix (f_{ctm}) is the major parameter controlling resistance against spalling. Therefore R_{SP1} becomes defined as following:

$$R_{SP1} = A_{SP1} \, f_{ctm} \tag{A2.2}$$

Where A_{SP1} is the thorough surface failure of the matrix wedge (Fig.A2.1) which is defined in Eqs.A2.3-A2.5.
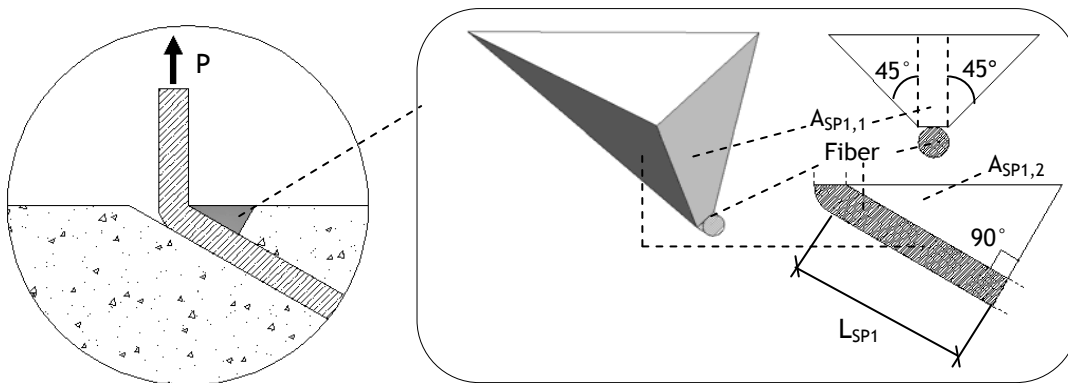

Fig.A2.1 – Geometry of the matrix wedge spalled off.

$$A_{SP1} = A_{SP1,1} + A_{SP1,2} \tag{A2.3}$$

$$A_{SP1,1} = L_{SP1} \frac{\cos\theta}{\sin\theta} \left(d + L_{SP1} \frac{\cos\theta}{\sin\theta} \right) \tag{A2.4}$$

$$A_{SP1,2} = L_{SP1}^2 \sqrt{2} \frac{\cos\theta}{\sin\theta} \qquad (A2.5)$$

The spalling force (F_{SP1}) is taken as the component of the deviation force (D_{F1}) parallel to the failure surface A_{SP1}, which according with experimental observations from Cailleux (2005) is also perpendicular to the fiber main axis (Fig.A2.2).
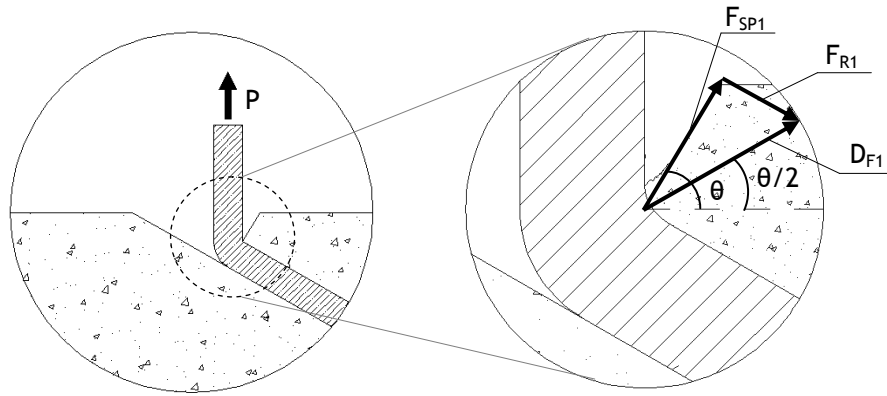

Fig.A2.2 - Schematic equilibrium of equivalent forces at fiber exit point.

Although the component of the deviation force parallel to the fiber main axis (F_{R1}) might introduce a sort of stabilization effect, due to the uncertainties on appropriately defining the stress field along the thorough matrix wedge it will be disregarded. Thereby the equivalent force which induces spalling on the matrix (F_{SP1}) becomes defined as following:

$$F_{SP1} = P_{S01} \sin\theta \cos\theta \qquad (A2.6)$$

Applying the failure criterion defined in Eq.A2.1 L_{SP1} becomes defined by simply solving a quadratic function $a.L_{SP1}^2+b.L_{SP1}+c=0$ with the parameters defined in Eqs.A2.7-A2.9.

$$a_1 = \frac{\sqrt{2}}{\sin\theta} + \frac{\cos\theta}{\sin^2\theta} \qquad (A2.7)$$

$$b_1 = \frac{d}{\sin\theta} \qquad (A2.8)$$

$$c_1 = -\frac{P_{S01} \sin\theta}{f_{ctm}} \qquad (A2.9)$$

A2.3   DEFINITION OF L$_{SP2}$

Following the methodology adopted in the previous section, the increment of spalled matrix along fiber axis (L$_{SP2}$) is calculated through a failure criterion between the new spalling force (F$_{SP2}$) and the resisting mechanism provided by the matrix wedge (R$_{SP2}$). Likewise L$_{SP2}$ represents the increment of spalled length at which the second stage of matrix spalling ceases, obtained by Eq.A2.10.

$$R_{SP2} \geq F_{SP2} \tag{A2.10}$$

The resisting mechanism provided by the matrix (R$_{SP2}$) is a very complex one, with tensile and shear stresses generating non-uniform and brittle failure surfaces. This approach assumes that the tensile strength of the matrix (f$_{ctm}$) is the major and unique parameter controlling resistance against spalling and that the tensile strength is attained uniformly over the failure surface, thus being defined by:

$$R_{SP2} = A_{SP2} \ f_{ctm} \tag{A2.11}$$

Where A$_{SP2}$ is the surface failure of the matrix wedge, defined in Eqs.A2.12-A2.14 and depicted in Fig.A2.3.

$$A_{SP2} = A_{SP2,1} + A_{SP2,2} \tag{A2.12}$$

$$A_{SP2,1} = \left(L_{SP1} + L_{SP2}\right) \frac{\cos\theta}{\sin\theta}\left[d + \left(L_{SP1} + L_{SP2}\right)\frac{\cos\theta}{\sin\theta}\right] \tag{A2.13}$$

$$A_{SP2,2} = L_{SP2} \ \sqrt{2} \ \frac{\cos\theta}{\sin\theta} \left(2 \ L_{SP1} + L_{SP2}\right) \tag{A2.14}$$
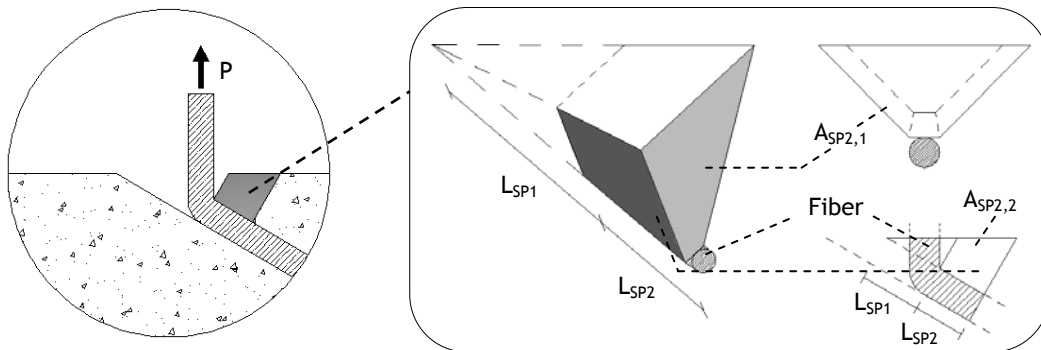
Fig.A2.3 – Geometry of the matrix wedge at the second stage of spalling.

Due to the increment of load carrying capacity provided by the hook an increased deviation force arises at the new fiber exit point, leading to the spalling force defined in Eq.A2.15.

$$F_{SP2} = P_{H01} \sin\theta \cos\theta \qquad \text{(A2.15)}$$

The increment of matrix spalled length (L_{SP2}) can then be calculated by solving a quadratic function $a.L_{SP2}^2 + b.L_{SP2} + c = 0$ with the following parameters:

$$a_2 = a_1 \qquad \text{(A2.16)}$$

$$b_2 = b_1 + \frac{2 L_{SP1} \left(\cos\theta + \sqrt{2} \right)}{\sin\theta} \qquad \text{(A2.17)}$$

$$c_2 = c_1 \frac{P_{H01}}{P_{S01}} + \frac{L_{SP1}}{\sin\theta} \left(d + L_{SP1} \frac{\cos\theta}{\sin\theta} \right) \qquad \text{(A2.18)}$$

Where a_1, b_1 and c_1 are the parameters of the analogous quadratic function used for the calculation of L_{SP1}.

Appendix 3

Inclined tensile strength and data for validation of the pullout model

A3.1   INTRODUCTION

In some cases, the load-crack width response of an inclined hooked steel fiber may be truncated due to the attainment of its ultimate load. The occurrence of such phenomenon significantly decreases the toughness of SFRC and, consequently, has to be considered when predicting the pullout responses of this type of fibers (Chapter 5).

The main goal of this appendix is to present a simple expression to estimate the inclined tensile strength of steel fibers. This way, fiber rupture could be avoided by choosing appropriate material properties in the design of SFRC. The heuristic method herein presented accounts for experimental data extracted from literature and assumes typical properties for current steel fibers in the market.

In the second part of this appendix, the input values used for the validation of the pullout model described in Chapter 5 are given in detail.

A3.2   PREDICTING $f_u(\theta)$

In the following, the inclined tensile strength of steel fibers is taken as the ratio between the ultimate pullout load of an inclined fiber and its respective cross-sectional area. This way, it is not a material property but rather a parameter that comprises all together tensile, shear and bending stresses.

To include $f_u(\theta)$ within the current approach a simplified heuristic procedure has been adopted. Firstly an inspection on the ultimate loads of steel fibers with different tensile strengths and pulled out at different inclination angles was performed to identify the magnitude and variations of the ultimate loads. For such purpose the experimental works on fibers with circular cross sections (Armelin and Banthia 1997; Van Gysel 2000; Cunha et al. 2007) were taken into account to evaluate the dependency of $f_u(\theta)$ with the inclination angles, fiber diameters, tensile strengths and testing configurations, such as shown in Tab.A3.1.

Table A3.1 – Ratios between inclined and aligned ultimate pullout loads at different inclination angles.

Reference	d	f_u	θ		
	[mm]	[MPa]	30°	45°	60°
van Gysel (2000)	0.50	2148		86%	81%
Armelin and Banthia (1997)	0.50	1150		86%	80%
Cunha et al. (2007)	0.75	1141	83%		72%
van Gysel (2000)	0.80	2117		80%	79%

The reduction of the ultimate loads at increasing inclination angles is clearly denoted in Tab.A3.1, whose values were reported with maximum coefficients of variation of about 5%. Such reduced scattering is of the same magnitude of the one observed in the aligned case, denoting a unique dependency on the properties of the fiber itself.

The main properties of commercial steel fibers currently in the market and used on previous research works were investigated and their typical properties are summarized in Tab.A3.2. Regarding such values an elastoplastic constitutive diagram for the tensile behavior of steel fibers can be idealized (Fig.A3.1). For simplicity the plastic range of the diagram ($\Delta\varepsilon_p$) is assumed to be constant and to comprehend two components, namely axial strain (ε_a) and fiber curvature (ε_c).

Table A3.2 – Typical properties of steel fibers.

Fiber elastic modulus (E_f)	200 GPa
Tensile yield strength (f_y)	1100/2100 MPa
Ultimate tensile strength (f_u)	(1.05 to 1.10) f_y
Ultimate strain (ε_u)	35‰
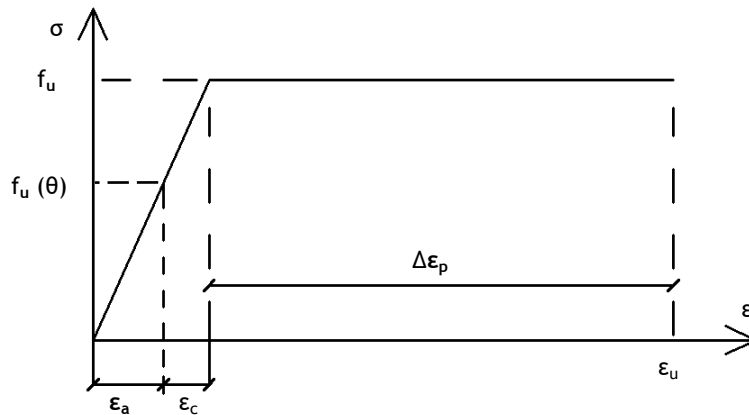
Fig.A3.1 – Assumed constitutive diagram for the tensile behavior of steel fibers

The radius of curvature of the fiber at failure (R_F) can then be idealized as an upper bound value due to material yielding (R_P) and a reduction component to account for the actual curvature at fiber exit point (R_C):

$$R_F = R_P - R_C \, \theta \tag{A3.1}$$

The first component of R_F is obtained through the aligned case (Eq.A3.2). The decrease in the radius of curvature with the inclination angle shall include the influence of fiber diameter and tensile strength. Furthermore it shall also consider the effect of testing configuration, regarding that single-sided pullout tests on inclined fibers require bending the fibers prior to testing, which tends to reduce the ultimate pullout loads. Therefore, according to the experimental data presented in Tab.A3.1, an empirical expression for R_C is proposed in Eq.A3.3.

$$R_P = \frac{d}{2\left(\dfrac{\varepsilon_u}{1000} - \dfrac{f_u}{E_f}\right)} \tag{A3.2}$$

$$R_C = k \, d \, f_u \, 10^{-6} \tag{A3.3}$$

With k being the parameter taking into account the pullout testing configuration, defined as following:

$$k = \begin{cases} 9 & \text{if fiber geometry is the original one prior to testing} \\ 18 & \text{if fiber is artificially deformed prior to testing} \end{cases} \tag{A3.4}$$

Taking into account Eqs.A3.1-A3.4 the inclined tensile strength of the steel fibers can then be approximated by Eq.A3.5:

$$f_u(\theta) = E_f \left(\frac{\varepsilon_u}{1000} - \frac{d}{2R_F} \right)$$ (A3.5)

It should be pointed out that this procedure is an approximation only valid for typical steel fibers and matrix properties such as the ones presented in Tab.A3.1, on fibers with circular cross-sections and with steel properties accordingly with Tab.A3.2. It is the author's opinion that, in the absence of improved predictive models, the inclined tensile strength shall be provided by the fibers' producers. In such scenario steel fibers should be tested under different inclination angles and without embedment on the matrix, according to the recommendations of other researchers (Bartos and Duris 1994). This way, given that matrix spalling relieves bending stresses due to decreasing curvatures at fiber exit points, this data would provide lower bound values for the ultimate tensile strength of inclined fibers.

A3.3   INPUT VALUES USED FOR MODEL VALIDATION

Table A3.3 – Input values used for model validation.

Reference		Robins et al. (2002)				van Gysel (2000)	
L_e	[mm]	20	15	10	5	30	30
d	[mm]		0.50			0.50	0.80
f_u	[MPa]		1150			2148	2117
f_{ctm}	[MPa]		4.46			4.57	
N	[-]		2			1	
k	[-]		9			18	
μ	[-]		0.6			0.6	
P_{S01}	[N]		25.0			105.0	203.0
w_{S01}	[mm]		0.035			0.104	0.134
P_{S02}	[N]		12.5			52.5	101.5
w_{S02}	[mm]		0.3			0.3	0.3
P_{H01}	[N]	192.0	183.6	175.0	66.9	321.2	743.9
w_{H01}	[mm]	0.769	0.800	0.600	0.590	0.965	0.853
P_{H02}	[N]	110	110	105	0	200	550
w_{H02}	[mm]	2.6	2.0	2.3	3.0	2.2	1.9
P_{H03}	[N]	90	110	90	0	170	550
w_{H03}	[mm]	4.5	3.5	4.0	3.0	3.5	3.8
P_{H04}	[N]	65	60	55	0	130	350
w_{H04}	[mm]	5.0	4.5	5.0	3.0	5.0	4.5

Appendix 4

Statistical analyses of the orientation profile

A4.1 INTRODUCTION

In Chapter 6 of this thesis, the orientation profile of SFRC was characterized by means of statistical analyses of individual fiber orientations. For that purpose, experimental data from literature was analyzed in detail. This chapter aims at providing detailed information of the statistical analyses carried out in 28 different cases.

First, the main features of the experimental data considered in this study are introduced. Then, the suitability of the statistical orientation laws investigated is presented for each case-study by means of the non-parametric test results and the coefficients of determination. Finally, comparisons between the orientation profiles of the Gumbel and the Gaussian distributions with the experimental data are presented.

A4.2 FEATURES OF THE EXPERIMENTAL DATA

Case	Fibers			Concrete matrix	
	Length	Diameter	Content	Average compressive strength	Maximum aggregate size
	[mm]	[mm]	[kg/m^3]	[MPa]	[mm]
1	30.5	0.39	40.0	70.3	8
2	20.2	0.31	60.0	75.6	8
3	41.2	0.64	100.0	73.5	16
4	28.8	0.62	140.0	78.1	16
5	61.1	0.71	60.0	75.1	16
6	30.5	0.39	60.0	72.3	16
7	30.5	0.39	60.0	57.6	16
8	61.1	0.71	60.0	54.0	16
9	28.8	0.62	140.0	55.8	16
10	41.2	0.64	100.0	51.9	16
11	61.1	0.71	60.0	75.3	16
12	28.8	0.62	140.0	71.7	16
13	61.1	0.71	60.0	116.6	16
14	51.1	1.06	50.0	*	*
15	51.1	1.06	50.0	*	*
16	51.1	1.06	50.0	*	*
17	51.1	1.06	50.0	*	*
18	51.1	1.06	50.0	*	*
19	51.1	1.06	50.0	*	*
20	60.0	0.75	20.0	70.6	12
21	60.0	0.75	20.0	70.6	12
22	60.0	0.75	20.0	70.6	12
23	60.0	0.75	20.0	70.6	12
24	60.0	0.75	20.0	70.6	12
25	60.0	0.75	20.0	70.6	12
26	60.0	0.75	20.0	70.6	12
27	60.0	0.75	20.0	70.6	12
28	60.0	0.75	20.0	70.6	12

Information not available

A4.3 RESULTS FROM THE NON-PARAMETRIC TESTS

Case	N	Δθ=10°				Δθ=15°			
		Gaussian		Gumbel		Gaussian		Gumbel	
		D(%)	p(λ)	D(%)	p(λ)	D(%)	p(λ)	D(%)	p(λ)
1	521	5.4	0.167	4.7	0.288	1.1	1.000	6.4	0.060
2	1038	3.1	0.296	3.5	0.190	2.3	0.685	3.8	0.123
3	430	6.3	0.148	2.8	0.961	4.3	0.588	2.8	0.961
4	659	9.2	0.000	6.4	0.027	9.2	0.000	6.0	0.042
5	345	9.1	0.217	5.8	0.759	9.1	0.217	5.8	0.759
6	707	6.6	0.011	3.5	0.445	4.3	0.213	3.1	0.619
7	659	1.6	0.999	4.0	0.371	2.2	0.957	5.0	0.144
8	195	7.8	0.287	2.0	1.000	5.6	0.703	1.9	1.000
9	628	5.0	0.181	5.2	0.148	4.1	0.384	4.9	0.206
10	434	5.5	0.202	4.9	0.327	5.4	0.230	5.4	0.221
11	314	5.4	0.338	3.4	0.866	5.4	0.338	4.4	0.613
12	818	7.7	0.001	5.3	0.045	7.7	0.001	3.1	0.541
13	266	4.6	0.990	1.7	1.000	4.4	0.995	1.4	1.000
14	142	6.1	0.668	12.8	0.019	6.1	0.668	12.8	0.019
15	139	4.1	0.971	9.9	0.134	3.9	0.984	9.9	0.134
16	85	5.1	0.980	7.4	0.747	5.2	0.977	7.4	0.747
17	93	6.5	0.833	6.3	0.855	6.5	0.833	8.0	0.587
18	48	8.6	0.870	16.0	0.170	3.6	1.000	11.6	0.536
19	92	5.8	0.918	9.6	0.362	5.8	0.918	7.7	0.650
20	320	7.6	0.051	5.8	0.240	5.0	0.408	5.8	0.240
21	198	9.7	0.047	13.2	0.002	8.7	0.098	12.3	0.005
22	168	6.3	0.521	9.6	0.089	4.8	0.827	9.6	0.089
23	320	13.6	0.000	18.9	0.000	9.7	0.005	17.4	0.000
24	198	21.0	0.000	26.8	0.000	21.0	0.000	28.5	0.000
25	168	7.3	0.326	12.8	0.008	6.4	0.493	11.3	0.028
26	320	11.2	0.001	17.5	0.000	11.6	0.021	17.2	0.000
27	198	10.5	0.026	17.1	0.000	9.8	0.044	17.1	0.000
28	168	11.6	0.021	19.3	0.000	11.6	0.021	19.3	0.000
Overall Acceptation levels		67.9%		64.3%		75.0%		67.9%	

Caption: N = Number of fibers

D= Maximum deviation between theoretical and experimental cumulative distributions.
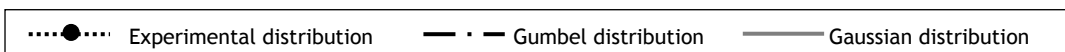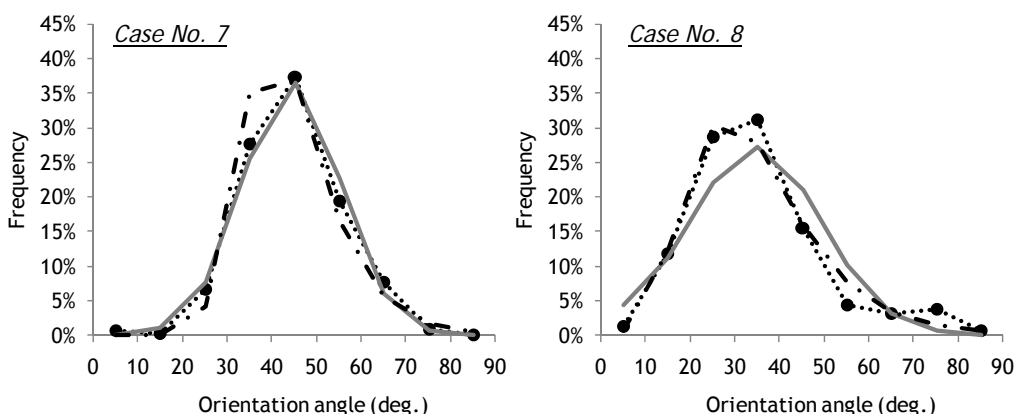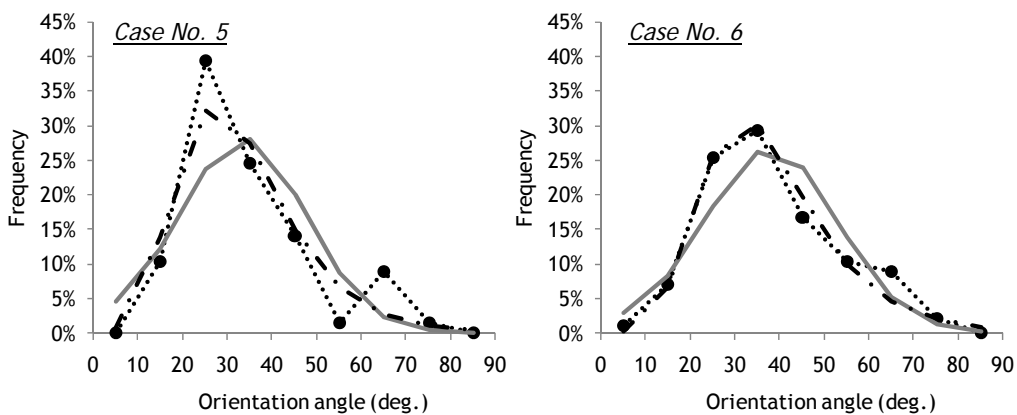
p(λ) = Parameter measuring the significance level (α)

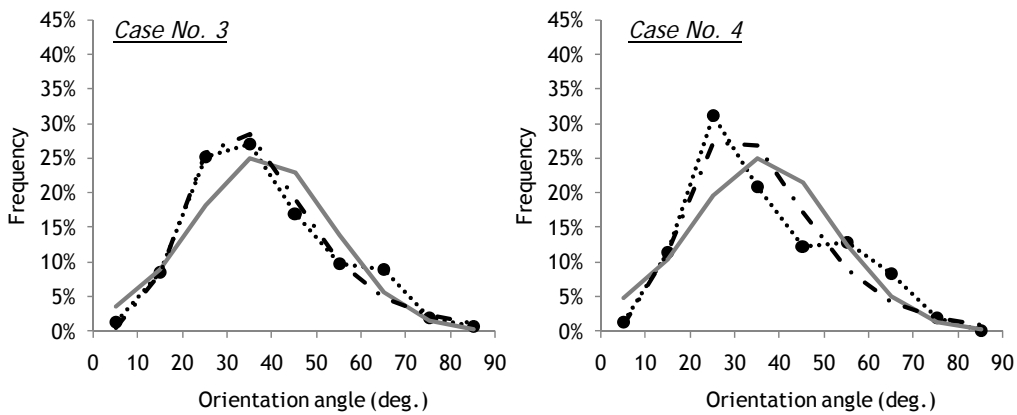Hypothesis $\begin{cases} \text{rejected if} & p(\lambda) < \alpha \\ \text{accepted if} & p(\lambda) \geq \alpha \end{cases}$ (α = 5%)

▓ Rejected hypothesis ☐ Accepted hypothesis

A4.4 COEFFICIENTS OF DETERMINATION (R^2)

Case	Direction	η_θ	$\Delta\theta=10°$ Gaussian (%)	Gumbel (%)	$\Delta\theta=15°$ Gaussian (%)	Gumbel (%)
1	X	0.74	92.6	95.9	99.6	94.4
2	X	0.72	94.4	95.3	97.3	95.1
3	X	0.76	84.9	97.8	87.7	98.9
4	X	0.78	68.5	88.0	71.6	87.9
5	X	0.81	71.4	90.7	73.1	93.1
6	X	0.77	84.2	97.2	89.2	98.0
7	X	0.70	98.7	96.3	98.3	96.9
8	X	0.80	87.5	97.2	88.5	99.5
9	X	0.75	87.9	93.4	93.3	96.6
10	X	0.77	83.5	95.9	88.0	95.3
11	X	0.80	92.0	97.9	90.7	96.8
12	X	0.79	73.0	92.5	77.8	96.0
13	X	0.81	90.1	99.0	91.7	99.6
14	Y	0.81	76.3	59.9	80.2	61.1
15	Y	0.79	87.8	75.5	92.5	69.5
16	Y	0.70	89.9	91.9	82.2	91.2
17	Y	0.74	89.6	89.2	96.3	89.4
18	Y	0.68	74.6	47.4	90.4	66.8
19	Y	0.69	86.4	81.8	95.7	90.8
20	X	0.70	53.6	86.2	63.3	94.7
21	X	0.64	0.1	12.8	2.5	21.8
22	X	0.65	68.1	86.7	75.3	90.3
23	Y	0.30	79.5	60.0	90.7	72.2
24	Y	0.28	60.1	36.7	66.3	41.1
25	Y	0.44	88.2	71.0	94.2	77.3
26	Z	0.47	69.4	41.2	63.4	36.4
27	Z	0.53	55.8	36.2	53.4	34.1
28	Z	0.43	62.1	31.3	61.5	28.8
Average direct. X			76.9	88.9	80.5	90.9
Average direct. Y			81.4	68.2	87.6	73.3
Average direct. Z			62.5	36.2	59.4	33.1
Overall			76.8	76.6	80.5	79.1

A4.5 STATISTICAL ORIENTATION LAWS (Δθ=10°)

Case No. 9 — Case No. 16: Frequency vs. Orientation angle (deg.) plots comparing Experimental distribution, Gumbel distribution, and Gaussian distribution.

Experimental distribution ⬤⬤⬤ — Gumbel distribution — · — Gaussian distribution

Experimental distribution ····•···· Gumbel distribution — · — Gaussian distribution ——

Case No. 25, Case No. 26, Case No. 27, Case No. 28
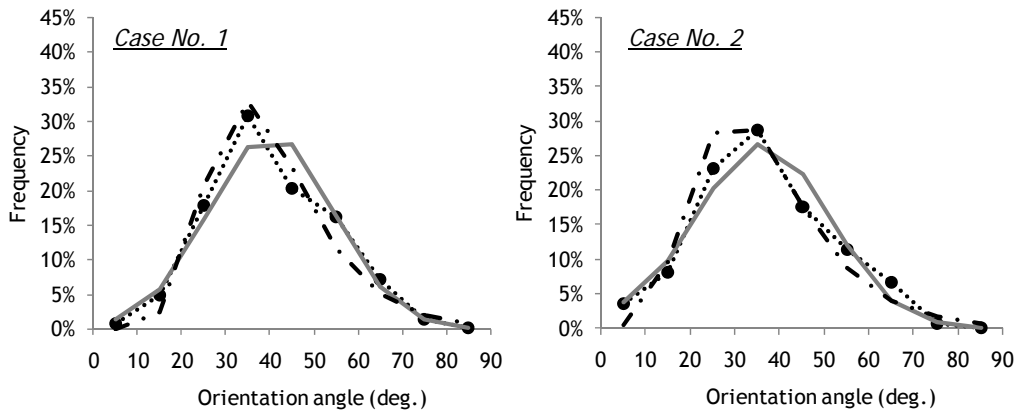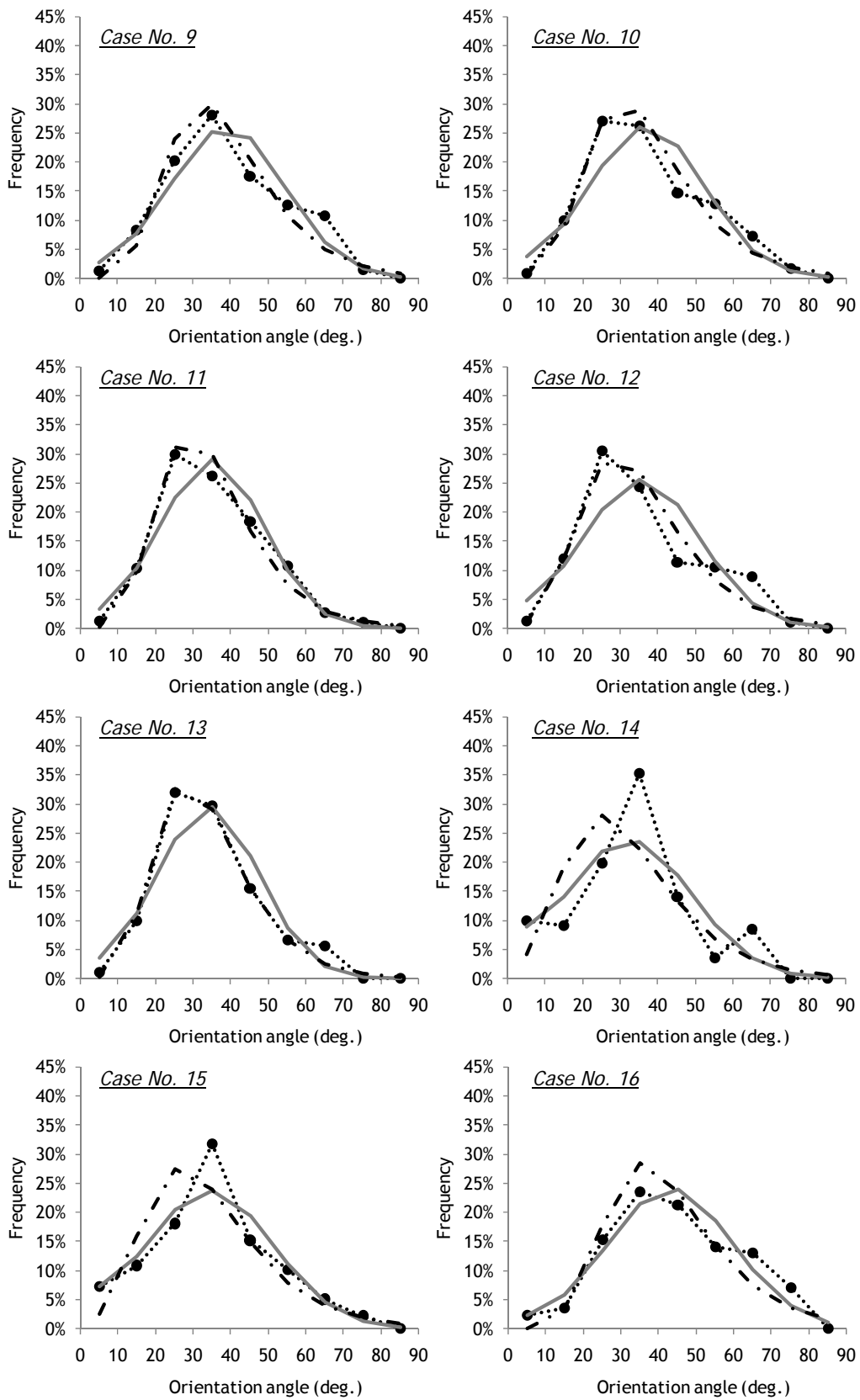
········●········ Experimental distribution   ─ · ─ Gumbel distribution   ───── Gaussian distribution
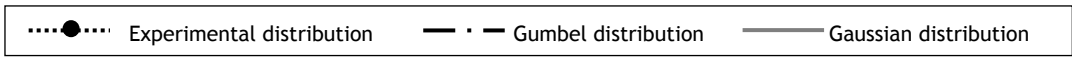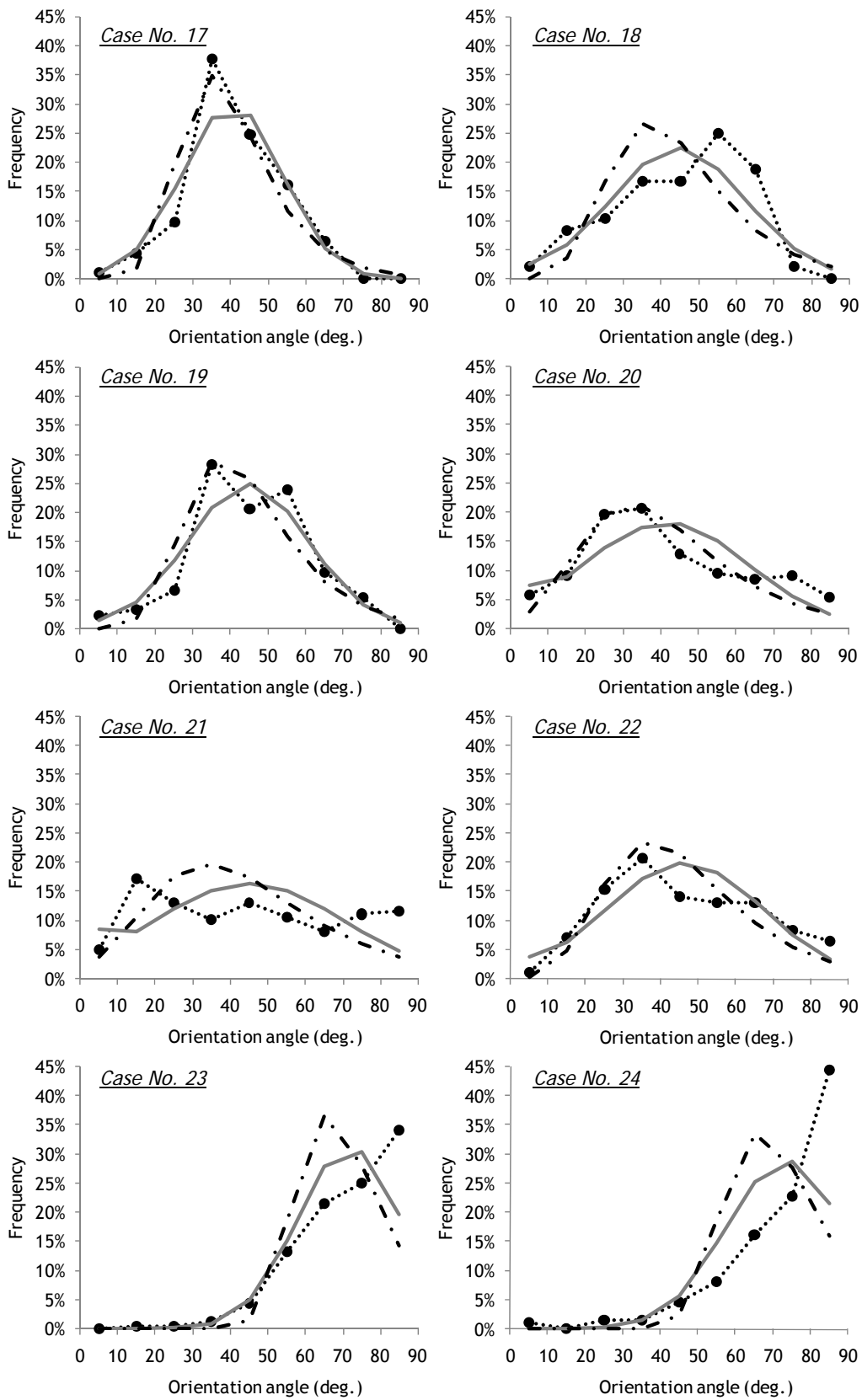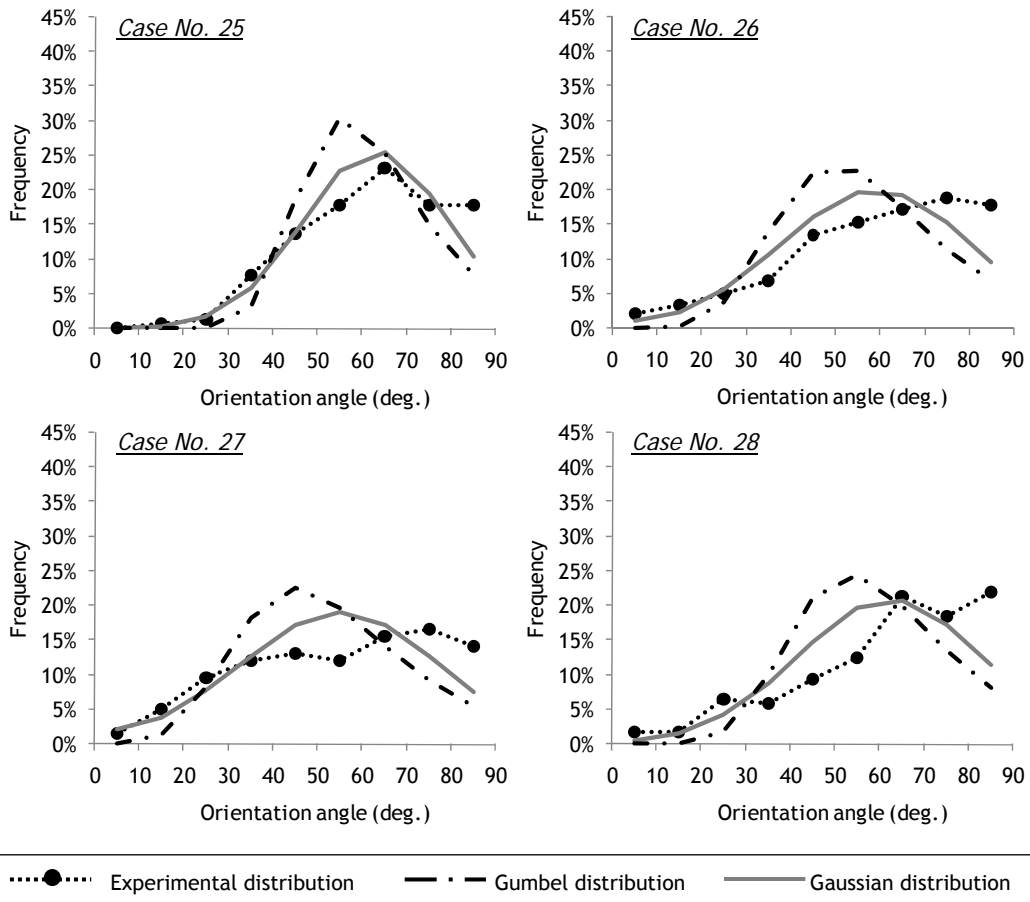
Appendix 5

Wall-effects on fiber orientation

A5.1   INTRODUCTION

This appendix supports the new framework to predict the orientation number of fibers advanced in Chapter 7. The influence of the wall-effects on fiber orientation is widely recognized. Nonetheless, because their quantification has always been done under the assumption of isotropic conditions in bulk, existing approaches have limited applicability. Regarding that SFRC tends to be anisotropic in nature, the quantification of the wall-effects for any orientation pattern in bulk should be possible.

Aiming to gain insight on the calculation of the orientation number, an alternative analytical formulation with regard to the ones existing in literature for isotropic conditions is presented in the first part of this appendix. Then, based on the approach to estimate the generalized wall-effects presented in Section 7.4.2, simplified expressions to quantify the wall-effects for any orientation number in the most common cross-section geometries are proposed.

A5.2   WALL-EFFECTS UNDER ISOTROPIC CONDITIONS

The orientation number (η) of a single fiber is the ratio between its projected length on a certain axis and its total length. When all the possible orientations of the fiber are considered, its end-points describe a spherical surface with radius (R) equal to half the fiber length. In isotropic conditions, all the points of the sphere have equal probability of occurrence. Thereby, η can be calculated as the ratio between the projected spherical surface along the considered axis (P_S) and the total spherical surface (A_S):

$$\eta = \frac{P_S}{A_S} \tag{A5.1}$$

A5.2.1 Orientation number of a fiber with one boundary condition

When fiber rotation capacity is restrained by one boundary condition (BC) its end-points describe a sphere that is cut by two symmetric sphere caps. Consider, for instance, that such BC is horizontal (Fig.A5.1a) and is located at a distance *h* from the fiber gravity point (Eq.A5.2). The vertical angle (φ) and the horizontal angle (α) will be considered in order to define the infinitesimal surface (*d*A), given by Eq.A5.3 (Fig.A5.1b):

$$h(\varphi_L) = \frac{L}{2} \times \sin \varphi_L \tag{A5.2}$$

$$dA = (R \times d\varphi) \times (r \times d\alpha) \tag{A5.3}$$

In Eq.A5.2, φ_L is the limit of the vertical angle up to which fiber is not influenced by the BC, whereas *r* (Eq.A5.3) is the horizontal projection of the spherical radius, defined in Eq.A5.4. Given that no vertical BC exist in this case, α is equal to β (horizontal angle in the plane xOz) and its limit value (α_L) in half-sphere is therefore π/2.

$$r = R \times \cos \varphi \tag{A5.4}$$

The available area of half-sphere in the presence of one BC parallel to xOz, $A_{S1}(\varphi_L)$, can then be defined by:

$$A_{S1}(\varphi_L) = \int_{\varphi=-\varphi_L}^{\varphi=\varphi_L} \int_{\alpha=-\frac{\pi}{2}}^{\alpha=\frac{\pi}{2}} dA = 2\pi R^2 \times \sin \varphi_L \tag{A5.5}$$

The respective projected surface along the x-axis (P_{S1}) is given in Eq.A5.7 in terms of its infinitesimal surface (*d*P):

$$dP = dA \times \cos \varphi \times \cos \alpha \tag{A5.6}$$

$$P_{S1}(\varphi_L) = \int_{\varphi=-\varphi_L}^{\varphi=\varphi_L} \int_{\alpha=-\frac{\pi}{2}}^{\alpha=\frac{\pi}{2}} dP = 2R^2 \times (\cos \varphi_L \times \sin \varphi_L + \varphi_L) \tag{A5.7}$$
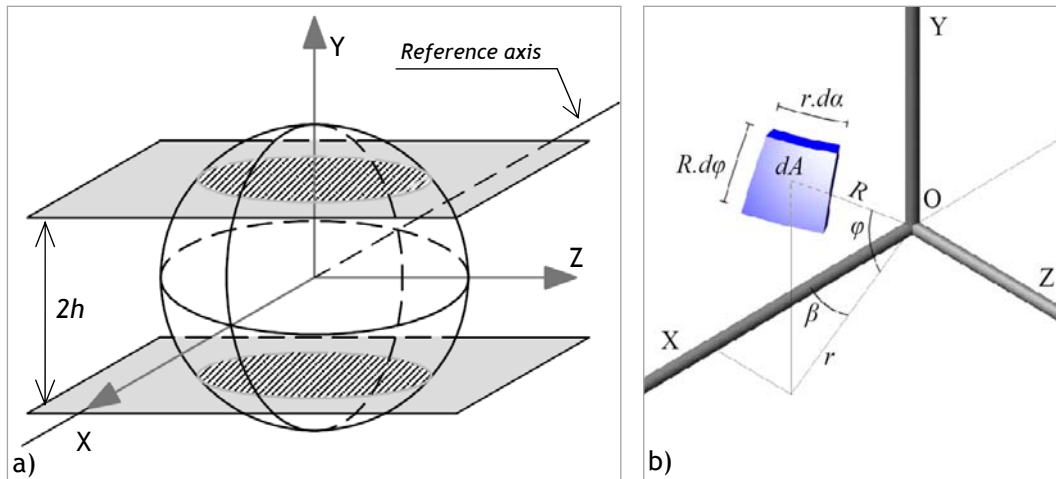
Fig.A5.1 - Fiber near one BC: a) Overview; b) Identification of main parameters.

The orientation number for one BC (η_1) parallel to xOz is then given by:

$$\eta_1(\varphi_L) = \frac{P_{S1}}{A_{S1}} = \frac{1}{\pi} \times \left(\cos\varphi_L + \frac{\varphi_L}{\sin\varphi_L} \right) \qquad \text{(A5.8)}$$

Given that the solution of Eq.A5.8 is a Bernoulli polynomial, the average η_1 along the bandwidth of influence of the wall requires numerical integration, returning:

$$\eta_1 = \int_{\varphi_L=0}^{\varphi_L=\frac{\pi}{2}} \eta_1(\varphi_L) \times d\varphi_L \approx 0.60 \qquad \text{(A5.9)}$$

In the absence of any BC, both α_L and φ_L would be equal to $\pi/2$ and, in that case, Eqs.A5.2-A5.9 would provide an average orientation number (η_0) equal to 0.50.

A5.2.2 Orientation number of a fiber with two boundary conditions

When a fiber is under the influence of two orthogonal BCs its end-points describe a sphere that is cut by two pairs of symmetric sphere caps (Fig.A5.2). The magnitude of the surfaces extracted by each pair of caps depends on the distance of the gravity point of the fiber (L_{GP}) to each of the walls. This way, two different scenarios may occur: either the pairs of sphere caps are independent between each other ($\beta_L+\varphi_L \geq \pi/2$) or they intersect themselves due to short proximity of L_{GP} to both walls ($\beta_L+\varphi_L < \pi/2$).

<u>Case 1</u>: Independent wall-effects ($\beta_L+\varphi_L \geq \pi/2$)

When the wall-effects of two BCs are independent from each other, the range of possible fiber orientations is defined accordingly with Fig.A5.2. Starting from the total spherical surface (Fig.A5.2a), the pairs of sphere caps referring to the wall parallel to xOz (Fig.A5.2b) and the one parallel to xOy (Fig.A5.2c) have to be extracted in order to obtain the portion of the spherical surface where fiber end-points can be located (Fig.A5.2d).
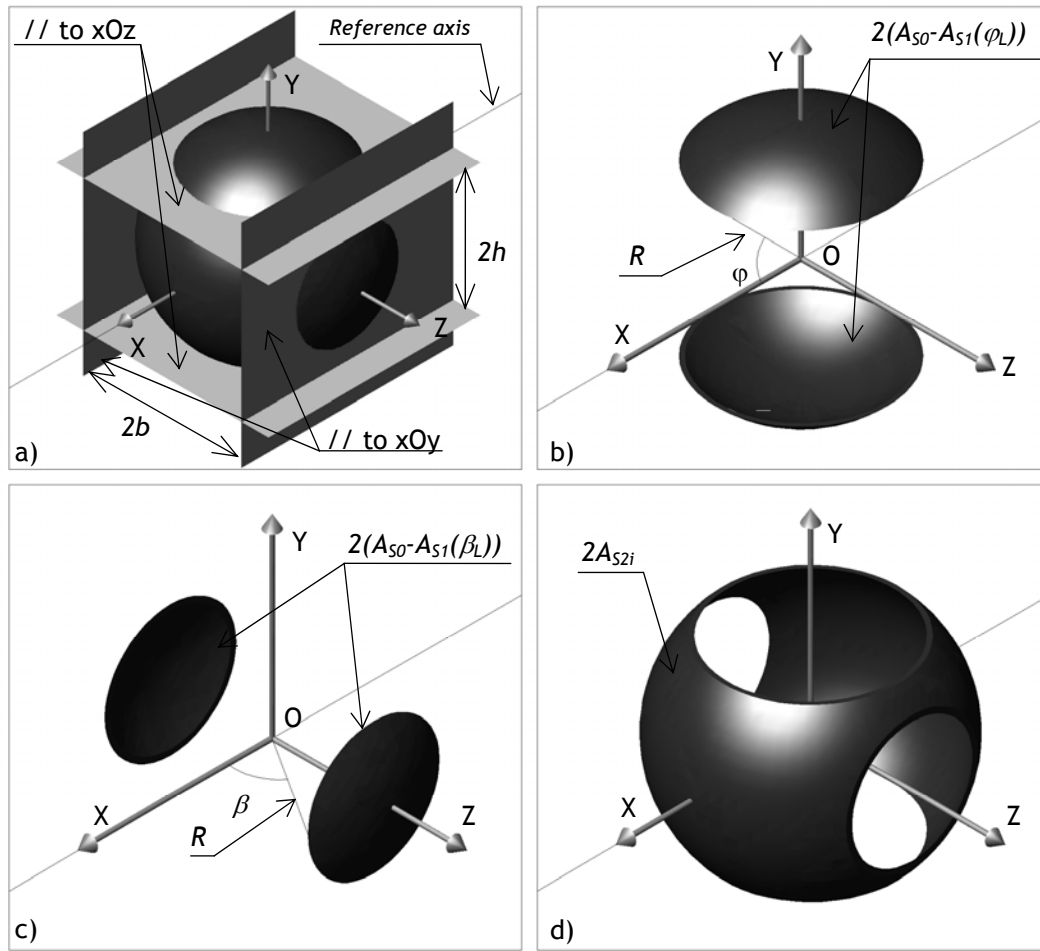
Fig.A5.2 - Fiber near a corner with two independent wall-effects.

The half of the total spherical surface (A_{S0}) and its respective projection along the x-axis (P_{S0}) can be obtained by fixing φ_L equal to $\pi/2$ in Eq.A5.5 and Eq.A5.7, respectively. $A_{S1}(\varphi_L)$ is the remaining surface of half-sphere after extraction of the sphere-cap parallel to the xOz plane and its respective projection in the x-axis is defined as $P_{S1}(\varphi_L)$. Similarly, $A_{S1}(\beta_L)$ is the remaining surface of half-sphere after extraction of the sphere-cap parallel to the xOy plane and its respective projection in the x-axis is defined as $P_{S1}(\beta_L)$. Note that in this case, α and β are no longer the same values and therefore Eq.A5.10 has to be considered for the limit angle α_L.

With the previous parameters, the total surface in the presence of two independent wall-effects A_{S2i} (Eq.A5.11), the respective projection in the x-axis, P_{S2i} (Eq.A5.12) and the respective orientation number, η_{2i} (Eq.A5.13) can be obtained:

$$\alpha_L = \operatorname{asin}\left(\frac{\sin \beta_L}{\cos \varphi}\right) \tag{A5.10}$$

$$\begin{aligned} A_{S2i}(\varphi_L, \beta_L) &= A_{S0} - \left(A_{S0} - A_{S1}(\varphi_L)\right) - \left(A_{S0} - A_{S1}(\beta_L)\right) \\ &= 2\pi R^2 \left(\sin \varphi_L + \sin \beta_L - 1\right) \end{aligned} \tag{A5.11}$$

$$P_{S2i}(\varphi_L, \beta_L) = P_{S0} - (P_{S0} - P_{S1}(\varphi_L)) - (P_{S0} - P_{S1}(\beta_L))$$
$$= 2R^2(\cos\varphi_L.\sin\varphi_L + \cos\beta_L.\sin\beta_L + \varphi_L + \beta_L) - \pi R^2 \tag{A5.12}$$

$$\eta_{2i} = \frac{P_{S2i}}{A_{S2i}} = \frac{2 \times (\cos\varphi_L.\sin\varphi_L + \cos\beta_L.\sin\beta_L + \varphi_L + \beta_L) - \pi}{2\pi \times (\sin\varphi_L + \sin\beta_L - 1)} \tag{A5.13}$$

<u>Case 2</u>: <u>Dependent wall-effects</u> ($\beta_L + \varphi_L < \pi/2$)

When the L_{GP} is at short distance to both of the orthogonal BCs, the extracted sphere caps from both walls superpose each other (Fig.A5.3a). Thereby, among the total amount of spherical fragments generated by the intersections with the walls (Fig.A5.3b), there is a reduced available surface where fiber end-points can be located (Fig.A5.3c). To calculate the orientation number of a fiber submitted to these two dependent wall-effects (η_{2d}) the infinitesimal surface dA (Eq.A5.3) has to be considered (Fig.A5.3d). Thereby, the available surface in the presence of two dependent wall-effects is given by:

$$A_{S2d} = \int_{\varphi=-\varphi_L}^{\varphi=\varphi_L} \int_{\alpha=-\alpha_L}^{\alpha=\alpha_L} dA$$
$$= 4R^2 \left[\sin\beta_L \times atan(K) - atan(\sin\beta_L \times K) + \sin\varphi_L \times asin\left(\frac{\sin\beta_L}{\cos\varphi_L}\right) \right] \tag{A5.14}$$

With K being a ratio of the distances between planes parallel to xOz and xOy:

$$K = \frac{\tan\varphi_L}{\sqrt{1 - \left(\frac{\sin\beta_L}{\cos\varphi_L}\right)^2}} \tag{A5.15}$$

And the respective projected surface in the x-axis (P_{S2d}) defined such as:

$$P_{S2d} = \int_{\varphi=-\varphi_L}^{\varphi=\varphi_L} \int_{\alpha=-\alpha_L}^{\alpha=\alpha_L} dP = 4R^2 \times \sin\varphi_L \times \sin\beta_L \tag{A5.16}$$

Consequently, the orientation number of a fiber subjected to two BCs with dependent wall-effects (η_{2d}) is given by:

$$\eta_{2d} = \frac{P_{S2d}}{T_{S2d}} = \frac{\sin\varphi_L \times \sin\beta_L}{\sin\beta_L \times atan(K) - atan(\sin\beta_L \times K) + \sin\varphi_L \times asin\left(\frac{\sin\beta_L}{\cos\varphi_L}\right)} \tag{A5.17}$$
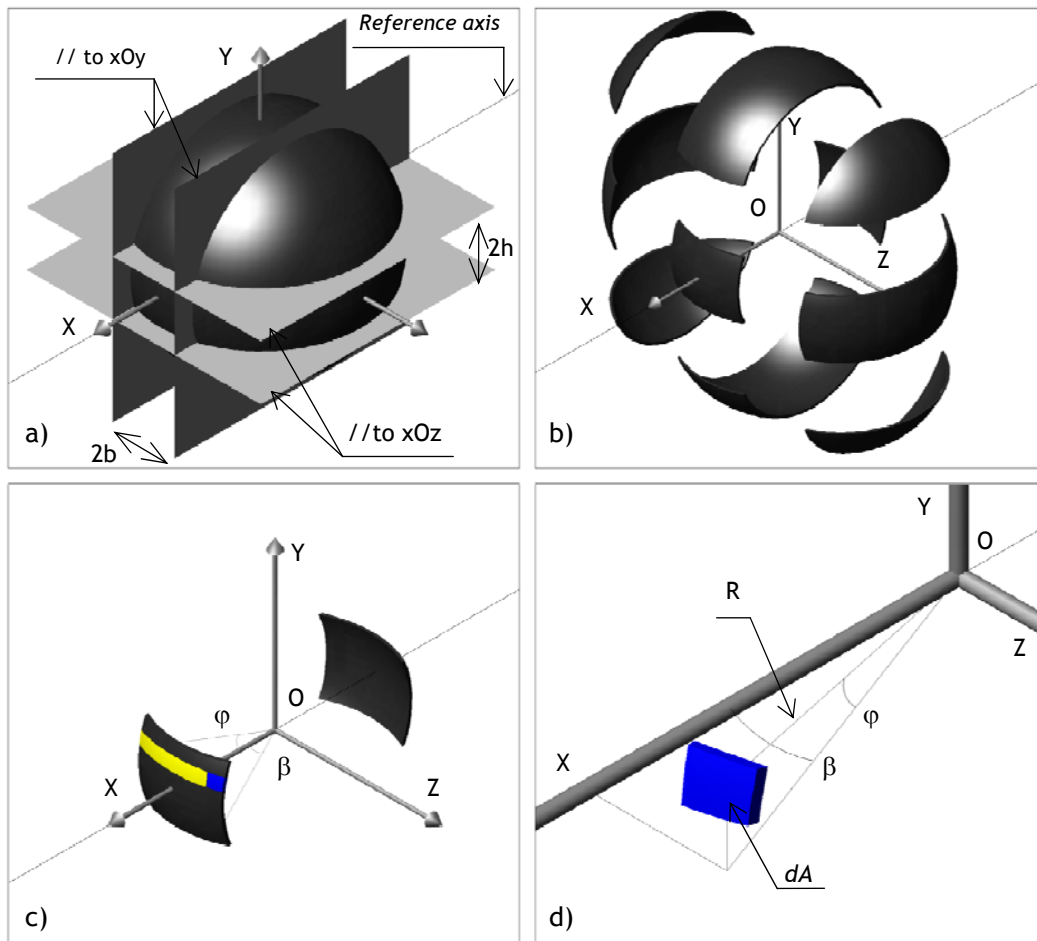
Fig.A5.3 - Fiber near a corner with two independent wall-effects.

<u>Average orientation number of a fiber with 2 BCs</u>

Once the orientation number of a fiber with 2 BCs is defined for the two possible scenarios previously defined, it can then be integrated along the bandwidth of influence of both walls to obtain the average orientation number (η_2):

$$\eta_2 = \int_{\varphi_L+\beta_L=0}^{\varphi_L+\beta_L=\frac{\pi}{2}} \eta_{2d} \times d\varphi_L \times d\beta_L \;+\; \int_{\varphi_L+\beta_L=\frac{\pi}{2}}^{\varphi_L+\beta_L=\pi} \eta_{2i} \times d\varphi_L \times d\beta_L \quad \approx 0.84 \tag{A5.18}$$

A5.3   GENERALIZED WALL-EFFECTS FOR COMMON CROSS-SECTION GEOMETRIES

The influence of the cross-section geometry on the average orientation of fibers can be quantified through the averaging procedure depicted in Fig.7.7. This way, the orientation number is simply defined by:

$$\eta = \frac{A_0 \times \eta_0 + A_1 \times \eta_1 + A_2 \times \eta_2}{A_0 + A_1 + A_2} \tag{A5.19}$$

Alternatively, η can also be obtained by adding to the average orientation in bulk (η_0) the respective increment due to the wall-effects for the entire cross-section, $\Delta\eta_W$ (Eq.A5.20). The latter is defined in Eq.A5.21 in terms of the average increments of the orientation number due to one BC ($\Delta\eta_1$) and two BCs ($\Delta\eta_2$). According to Eqs.A5.19-A5.21, $\Delta\eta_1$ and $\Delta\eta_2$ can be quantified uniquely in terms of η_0, such as shown in Eqs.A5.22-23, respectively.

$$\eta = \eta_0 + \Delta\eta_W \tag{A5.20}$$

$$\Delta\eta_W = \frac{A_1 \times \Delta\eta_1 + A_2 \times \Delta\eta_2}{A_0 + A_1 + A_2} \qquad (\geq 0) \tag{A5.21}$$

$$\Delta\eta_1 = \eta_1 - \eta_0 \qquad (\geq 0) \tag{A5.22}$$

$$\Delta\eta_2 = \eta_2 - \eta_0 \qquad (\geq 0) \tag{A5.23}$$

Regarding Eqs.A5.19-23, the quantification of the wall-effects can be generalized for any η_0 through simple and straightforward expressions for the most common cross-section geometries. However, in the case of SCC, the wall-effects introduced by horizontal BCs may be negligible given the intrinsic tendency of fibers to align in horizontal planes. Thereby, $\Delta\eta_W$ of SCC depends on whether the cross-section is contained or not in the vertical plane. When the latter occurs, the assumption previously advanced for the fresh-state properties of SCC implies a distance between horizontal boundaries (H) equal to the fiber length (L). Consequently, η_0 becomes equal to η_1 and the values obtained from Eqs.A5.22-23 provide simpler expressions.

A5.3.1 Rectangular cross-section

According to Fig.7.7, the sub-areas A_0, A_1 and A_2 of a rectangular cross-section are defined uniquely in terms of its width (B), height (H) and fiber length (L):

$$A_0 = (B - L) \times (H - L) \qquad (\geq 0) \tag{A5.24}$$

$$A_1 = (B - L) \times L + (H - L) \times L \qquad (\geq 0) \tag{A5.25}$$

$$A_2 = L^2 \qquad (\geq 0) \tag{A5.26}$$

Introducing Eqs.A5.22-26 in Eq.A5.21, $\Delta\eta_W$ can then be obtained for CC:

$$\Delta\eta_W = \frac{L^2}{B \times H}\left[\frac{B + H}{L}(0.465 - 0.730\eta_0) + 0.533\eta_0 - 0.127\right] \tag{A5.27}$$

In case of SCC, Eq.A5.27 applies whenever the tendency of fibers towards horizontal orientations does not influence the wall-effects (cross-sections in horizontal plane). On the other hand, for cross-sections in the vertical plane, a simplified expression is obtained given that an intrinsic horizontal BC is being assumed for SCC in bulk. Hence, only the vertical walls play major influence (Eq.A5.28). This will occur for any geometry considered for the cross-section.

$$\Delta\eta_W = \frac{L}{B} \times \left(0.677 - 0.73 \times \eta_0\right)$$
(A5.28)

A5.3.2 Circular cross-section

Cross-sections with circular geometry can be subdivided in two zones, with zero and one BCs (A_0 and A_1, respectively), as shown in Fig.A5.4a. These sub-areas are defined by Eq.A5.29 and Eq.A5.30, respectively:

$$A_0 = \frac{\pi}{4} \times \left(D - L^*\right)^2 \qquad \left(\geq 0\right)$$
(A5.29)

$$A_1 = \frac{\pi}{4} \times L^* \left(2 \times D - L^*\right) \qquad \left(\geq 0\right)$$
(A5.30)

Adding Eqs.A5.21-23 and Eqs.A5.29-30, $\Delta\eta_W$ can be simply defined by:

$$\Delta\eta_W = \frac{L^* \times \left(2D - L^*\right)}{D^2} \times \left(0.465 - 0.730\eta_0\right)$$
(A5.31)

However, in case of vertical cross-sections with SCC, $\Delta\eta_W$ is obtained by:

$$\Delta\eta_W = \frac{L^* \times \left(2D - L^*\right)}{D^2} \times \left(0.677 - 0.730\eta_0\right)$$
(A5.32)

Due to the curved shape of the walls in circular cross-sections, the gravity-point of the fiber no longer reaches the BC because fiber end-points are restrained in their rotation ability. This phenomenon is herein defined as the "chord-effect" (Fig.A5.4b) and, for practical purposes, it implies an increment of the bandwidth of influence of the BC (ΔL) which is then provided in terms of a corrected fiber length (L^*):

$$L^* = L + \Delta L$$
(A5.33)

According to its mathematical definition (A5.34), the chord of an angle θ is the length of the chord between two points on a unit circle separated by that angle. Regarding Fig.A5.4b, it can be seen that this chord corresponds to the fiber length (A5.35) and, consequently, the angle to the center (θ) can be obtained (Eq.A5.36).

$$\text{chord}(\theta) = 2 \times \sin\left(\frac{\theta}{2}\right)$$
(A5.34)

$$L = \text{chord}(\theta) \times \frac{D}{2}$$
(A5.35)

$$\theta = 2 \times \sin\left(\frac{L}{D}\right) \tag{A5.36}$$

The maximum distance between the fiber and the curved wall (ΔL') is, by definition, equal to:

$$\Delta L' = \frac{D}{2} \times \left[1 - \cos\left(\frac{\theta}{2}\right)\right] \tag{A5.37}$$

Regarding Eqs.A5.36-37 and the fact that ΔL' has to be considered twice for the whole cross-section, ΔL thus returns:

$$\Delta L = D \times \left[1 - \cos\left(a\sin\left(\frac{L}{D}\right)\right)\right] \tag{A5.38}$$

It should be noted that when D >> L, then ΔL* ≈ 0 and, consequently, the chord-effect is negligible. On the other hand, if D is not much larger than L, neglecting Eq.A5.38 underestimates the overall orientation number. For instance, for a cross-section with 150mm diameter and fibers with 60mm length (Fig.A5.4), the value of $\Delta\eta_W$ without considering the chord-effect is approximately 13% lower.
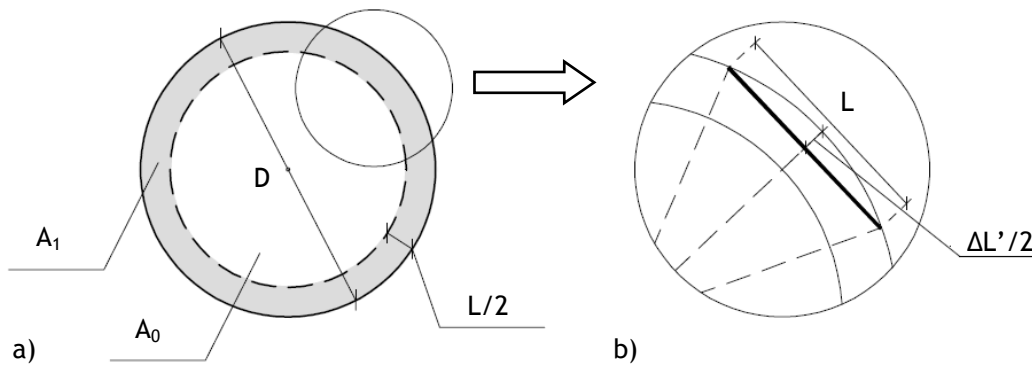
Fig.A5.4 Circular cross-section: a) Sub-areas; b) Detail of the "chord-effect".

A5.3.3 Hollow-circular cross-section

This type of cross-section geometries can be subdivided in two zones, with zero and one BCs (A_0 and A_1, respectively), as shown in Fig.A5.5a. Both A_1 (Eq.A5.39) and the sum of A_1 with A_0 (Eq.A5.40) can be defined in terms of the external and internal diameters (D_e and D_i, respectively):

$$A_1 = \frac{\pi}{4} \times L \times (D_i + D_e) \qquad (\geq 0) \tag{A5.39}$$

$$A_1 + A_0 = \frac{\pi}{4} \times (D_e^2 - D_i^2) \qquad (\geq 0) \tag{A5.40}$$

Adding Eqs.A5.21-23 and Eqs.A5.39-40 and considering the thickness of the cross-section (T) as the difference between D_e and D_i, $\Delta\eta_W$ can then be defined by:

$$\Delta\eta_W = \frac{L}{T} \times (0.465 - 0.730\eta_0)$$

(A5.41)

However, in case of vertical cross-sections with SCC, $\Delta\eta_W$ is obtained by:

$$\Delta\eta_W = \frac{L^* \times (2D - L^*)}{D^2} \times (0.677 - 0.730\eta_0)$$

(A5.42)

In contrast with circular cross-sections, the chord-effect was not introduced in Eqs.A5.41-42. This occurs because, as shown in Fig.A5.5b, the increment of bandwidth introduced by the external wall is balanced by an approximately similar reduction inferred by the internal wall.
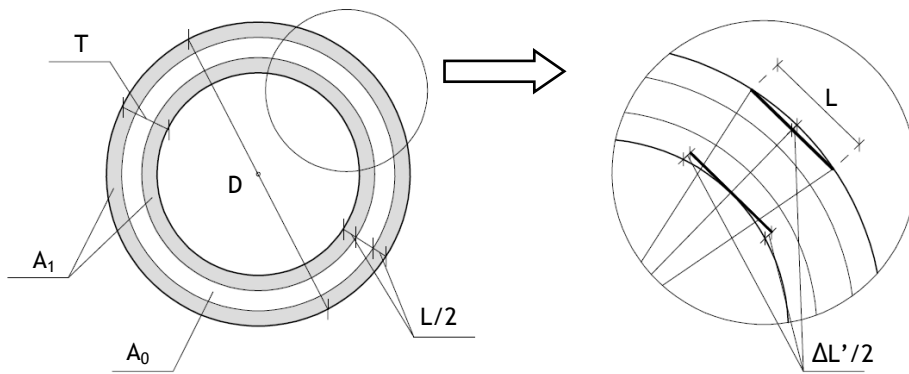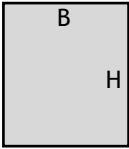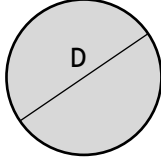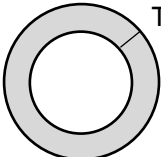
Fig.A5.5 Hollow-circular cross-section: a) Sub-areas; b) Balanced "chord-effect".

A5.3.4 Summary

Table A5.1 Increments of η for any η₀ and common cross-section geometries.

Cross-section		Type of concrete	Increment of η due to wall-effects ($\Delta\eta_w$)
Geometry	**Position**		
<u>Rectangular</u> B H B = Width H = Height L = Fiber length	Vertical	SCC	$\Delta\eta_w = \dfrac{L}{B} \times (0.677 - 0.730 \times \eta_0)$
		CC	$\Delta\eta_w = \dfrac{L^2}{B \times H}\left[\dfrac{B+H}{L}(0.465 - 0.730\eta_0) + 0.533\eta_0 - 0.127\right]$
	Horizontal or Inclined	SCC	
		CC	
<u>Circular</u> D D = Diameter L = Fiber length	Vertical	SCC	$\Delta\eta_w = \dfrac{L^* \times (2D - L^*)}{D^2}(0.677 - 0.730\eta_0)$
		CC	$\Delta\eta_w = \dfrac{L^* \times (2D - L^*)}{D^2}(0.465 - 0.730\eta_0)$
	Horizontal or Inclined	SCC	
		CC	
			$L^* = L + \Delta L$ $\Delta L = D \times \left[1 - \cos\left(a\sin\left(\dfrac{L}{D}\right)\right)\right]$
<u>Hollow-circular</u> T T = Thickness L = Fiber length	Vertical	SCC	$\Delta\eta_w = \dfrac{L}{T}(0.677 - 0.730\eta_0)$
		CC	$\Delta\eta_w = \dfrac{L}{T}(0.465 - 0.730\eta_0)$
	Horizontal or Inclined	SCC	
		CC	

NOTE: When calculating $\Delta\eta_{CW}$, if concrete is poured with free top-surface:

$$H = H_{c,eff} = \begin{cases} \min\{2 \times H_c, L\} & \text{if SCC} \\ 2 \times H_c & \text{if CC} \end{cases}$$

Appendix 6

Experimental validation of the framework to predict fiber orientation

A6.1   INTRODUCTION

A new framework to predict the orientation number of fibers was advanced in Chapter 7 by taking into account the combined influence of material properties, production processes and the geometry of the structure. Regarding the novelty of the proposed approach, experimental data from three different research works were considered for its validation.

The objective of this appendix is to provide details on how the overall results presented in section 7.6.3 were obtained. In this way, the experimental input values used for validation of the proposed framework are summarized. Then, for the sake of clarity, the results from the application of the proposed framework are presented step-by-step up to the final orientation numbers in the hardened state for all the 34 cases investigated.

A6.2   INPUT DATA FOR EXPERIMENTAL VALIDATION

Table A6.1 – Experimental data used for validation of the proposed framework.

Ref.	Case	Fiber		Casting method				Formwork	
		Characteristics		Direction		Geometry		Geometry	
		L	d	φ	β	B_C	$H_{C,eff}$	B_F	H_F
		[mm]	[mm]	[deg.]	[deg.]	[mm]	[mm]	[mm]	[mm]
[14]	1	30.5	0.39				30.5		
	2	20.2	0.31				20.2		
	3	41.2	0.64				41.2		
	4	28.8	0.62				28.8		
	5	61.1	0.71				60.0		
	6	30.5	0.39				30.5		
	7	30.5	0.39	45	45	60	30.5	150	150
	8	61.1	0.71				60.0		
	9	28.8	0.62				28.8		
	10	41.2	0.64				41.2		
	11	61.1	0.71				60.0		
	12	28.8	0.62				28.8		
	13	61.1	0.71				60.0		
	14	13.0	0.16				13.0		
[34]	15								
	16								
	17								
	18								
	19	30	0.375	90	*	**	**	150	300
	20								
	21								
	22								
	23								
	24								
[20]	25	6	0.16				6		
	26								
	27	13	0.20				13		
	28								
	29			≈ 0	0	60		150	150
	30								
	31								
	32	60	0.70				60		
	33								
	34								

*   Indifferent

** Very large number (Influence of the casting element is assumed to be negligible)

A6.3   RESULTS FROM EXPERIMENTAL VALIDATION

Table A6.2 – Detailed results from the experimental validation.

Case	η_{Mx}	$\Delta\eta_{Cx}$			$\Delta\eta_{Dx}$		$\Delta\eta_{FWx}$	$\eta_{\theta x}$		Absolute deviation
		η_{C0}	$\Delta\eta_{CW}$	C_{Dx}	$\Delta\eta_{DVx}$	$\Delta\eta_{DFx}$		Predicted	Exp.	
1			0.243	0.331			0.037	0.717	0.741	3.2%
2			0.201	0.374			0.025	0.700	0.721	2.9%
3			0.286	0.296			0.049	0.734	0.763	3.9%
4			0.236	0.338			0.035	0.714	0.779	8.3%
5			0.372	0.250			0.070	0.763	0.813	6.2%
6			0.243	0.331			0.037	0.717	0.765	6.3%
7	0.600	0.474	0.243	0.331	0.0	0.0	0.037	0.717	0.704	1.9%
8			0.372	0.250			0.070	0.763	0.800	4.7%
9			0.236	0.338			0.035	0.714	0.751	4.9%
10			0.286	0.296			0.049	0.734	0.774	5.2%
11			0.372	0.250			0.070	0.763	0.799	4.5%
12			0.236	0.338			0.035	0.714	0.787	9.2%
13			0.372	0.250			0.070	0.763	0.810	5.8%
14			0.172	0.411			0.016	0.687	0.715	3.9%
15									0.682	5.0%
16									0.709	8.6%
17									0.705	8.1%
18									0.676	4.2%
19	0.600	0.300	0.246	0.000	0.0	0.00	0.048	0.648	0.694	6.7%
20									0.706	8.2%
21									0.679	4.6%
22									0.684	5.3%
23									0.703	7.9%
24									0.649	0.2%
25			0.049				0.008	0.657	0.596	10.3%
26									0.637	8.5%
27			0.075				0.016	0.691	0.691	0.1%
28									0.703	1.6%
29									0.721	4.1%
30	0.600	0.600		1.000	0.0	0.0			0.912	4.3%
31									0.921	5.2%
32			0.251				0.022	0.873	0.853	2.3%
33									0.862	1.3%
34									0.770	13.4%
								Average deviation		**5.3%**

Appendix 7

Literature survey on pullout test results of aligned fibers

A7.1   INTRODUCTION

In part III of this thesis, two predictive models for the pullout response of inclined steel fibers were advanced. In both approaches, the prediction of the load-crack width diagrams of inclined fibers was done by taking into account experimental data characterizing the bond-strength between a specific combination of steel fibers and concrete mixture.

Most of the times the load-carrying capacity of a steel fiber perpendicular to the cracked surface under uniaxial tension is unknown, which would hinder the application of the new constitutive model. In order to avoid this from happening, experimental pullout test results of aligned straight and hooked steel fibers reported in literature is herein presented. Then, some correlations between the properties of the constituent materials and the experimental data collected are advanced.

The objective of this appendix is to provide a first order of magnitude for the experimental key-points needed to apply the new constitutive model.

A7.2   STRAIGHT STEEL FIBERS

In order to define the pullout responses of inclined straight fibers it is necessary to characterize the interface properties between fibers and the cementitious matrix. According to Eq.4.1, the peak load (P_{S01}) depends on the fiber diameter, fiber embedded length and on the apparent interfacial shear stress (τ^*). The later reflects the properties of the microstructure at the interfacial transition zone and, therefore, it is expected that larger values τ^* may occur in the presence of concrete matrices with improved mechanical properties. This way, a correlation between τ^* and f_{ctm} will be proposed in the following. For that purpose, consider the experimental data from literature summarized in Table A7.1.

Table A7.1 – Experimental data reported in literature from pullouts of aligned straight fibers.

Reference	f_{cm} [MPa]	f_{ctm} [MPa]	L_e [mm]	d [mm]	f_y [MPa]	P_U [N]	P_{S01} [N]
Ouyang et al. (1994)	57.8	4.06	12	0.41	1803	238.0	40.3
Van Gysel (2000)	47.4	3.5	30.0	0.50	1200	235.6	80.8
				0.80	1200	603.2	190.4
				0.50	2100	412.3	72.4
				0.80	2100	1055.6	104.1
	76.5	4.6	30.0	0.50	1200	235.6	126.6
				0.80	1200	603.2	142.1
				0.50	2100	412.3	105.0
				0.80	2100	1055.6	203.0
Cunha et al. (2007)	83.4	4.7	20	0.75	1100	486.0	77.4
			30	0.75	1100	486.0	155.0
Blázquez (2009)	22.1	1.8	30	0.75	2000	884	65.9

The data from Table A7.1 supports the evidence that, due to the low bond strength that tends to exist between straight fibers and the surrounding matrix, the maximum pullout loads (P_{S01}) are likely much smaller than their ultimate loads (P_U). The ratios between the maximum and the ultimate pullout loads reported in Table A7.1 are correlated with the respective theoretical ratios in Fig.A7.1. These theoretical ratios were calculated through Eq.4.1 on the basis of apparent interfacial shear stress (τ^*) equal to the matrix tensile strength (f_{ctm}).

Despite the large sensitivity that characterizes the debonding process of straight fibers, Fig.A7.1 shows that an approximated linear correlation may exist between the experimental and the theoretical peak loads of aligned fibers. In other words, this means that τ^* may vary linearly with f_{ctm}. Thereby, considering Eq.4.1 and the correlation shown in Fig.A7.1, P_{S01} can be roughly approximated by Eq.A7.1.
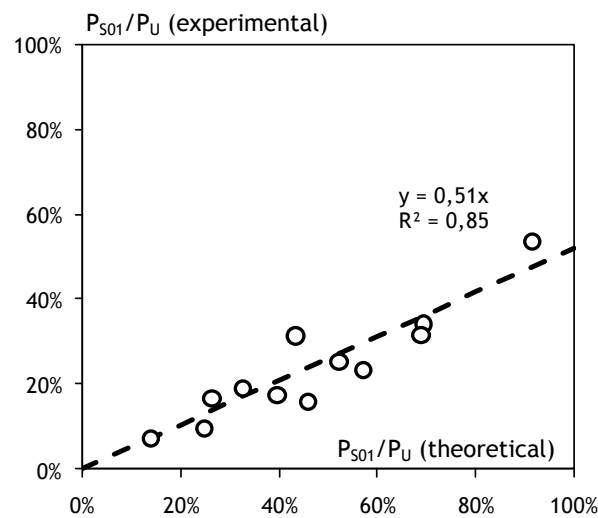
Fig.A7.1 – Ratios between maximum and ultimate pullout loads for straight steel fibers.

$$P_{S01} \approx \pi \times d \times L_e \times (0.51 \times f_{ctm}) \tag{A7.1}$$

A7.3 HOOKED STEEL FIBERS

According to Chapter 5, the pullout responses of aligned hooked steel fibers within a crack-width range up to 3.5mm can be approximated by three key-points: P_{S01}, P_{H01} and P_{H04}. While the former may be approximated by Eq.A7.1, the pullout loads at peak (P_{H01}) and at the post-peak (P_{H04}) may also be correlated with specific properties of the fibers and the matrix. For that purpose, consider the experimental data from literature summarized in Table A7.2.

Table A7.2 - Experimental data reported in literature from pullouts of aligned hooked fibers.

Reference	f_{cm}	f_{ctm}	L_e	d	f_y	P_U	P_{H01}	P_{H04}
	[MPa]	[MPa]	[mm]	[mm]	[MPa]	[N]	[N]	[N]
Banthia and Trottier (1994)	40.0	3.0	30	0.80	1115	560.5	273.0	200.0
Armelin and Banthia (1997)	58.0	4.1	15	0.50	1150	225.8	165.0	50.0
Robins et al. (2002)	72.0	4.5	20	0.50	1150	225.8	192.0	65.0
			15	0.50	1150	225.8	183.6	60.0
			10	0.50	1150	225.8	175.0	55.0
Blazquéz (2009)	63.5	4.2	30	0.75	2000	883.6	390.7	248.9
	53.5	3.8	30	0.75	2000	883.6	406.4	241.1
	44.6	3.3	30	0.75	2000	883.6	353.6	156.1
	20.2	1.6	30	0.75	2000	883.6	183.9	97.7

From Table A7.2 it can be seen that, contrarily to straight fibers, the ratios between the maximum and ultimate pullout loads of hooked fibers can be rather larger. This explains both the higher performance denoted by these type of fibers on improving the crack-bridging capacity of SFRC as well as the higher proneness to the occurrence of fibers rupture during the pullout process.

The maximum pullout load of aligned hooked fibers (P_{H01}) reflects the level of plastic deformations occurring at the zone of the hook: large peak loads occur when the straightening process of the hook is larger. The energy required to deform the fiber increases with its diameter. Moreover, it also increases with the capacity of the matrix on providing a rigid medium that forces the hook to slip along its narrow channel. Thereby, it may be reasonable to assume that P_{H01} is somehow dependent on the ratio between the matrix tensile strength (f_{ctm}) and the fiber tensile yield strength (f_y). The reasonableness of this assumption is proved in Fig.A7.2 which compares the ratio between f_{ctm} and f_y with the one obtained from the maximum and ultimate pullout loads extracted from Table A7.2.
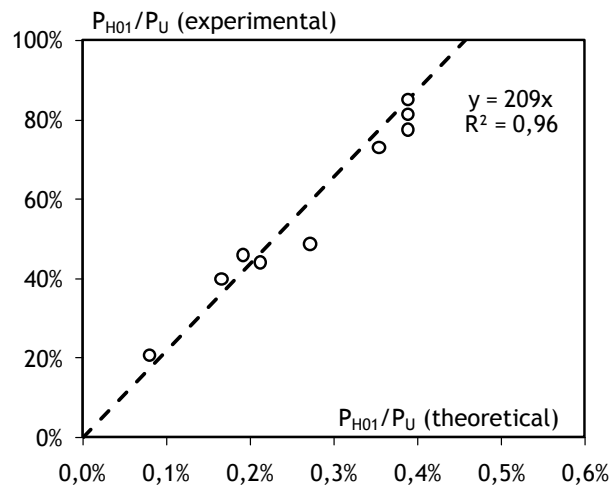
Fig.A7.2 – Ratios between maximum and ultimate pullout loads of hooked fibers.

Given the correlation presented in Fig.A7.2, P_{H01} may be approximated as follows:

$$P_{H01} \approx 209 \times A_f \times f_{ctm} \qquad\qquad (A7.2)$$

The pullout load after the straightening of the hooked-end (P_{H04}) depends uniquely on friction effects. The better the quality of the matrix, the larger should be the resistance provided against fiber slippage. Thereby, P_{H04} is expected to be proportional to f_{ctm} and, considering Eq.A7.2, also to P_{H01}. Fig.A7.3 shows the ratios between P_{H01} and P_{H04} from the experimental data reported in Table A7.2. From the correlation that is pointed out in Fig.A7.3, P_{H04} can then be approximated in terms of the peak load through Eq.A7.3.
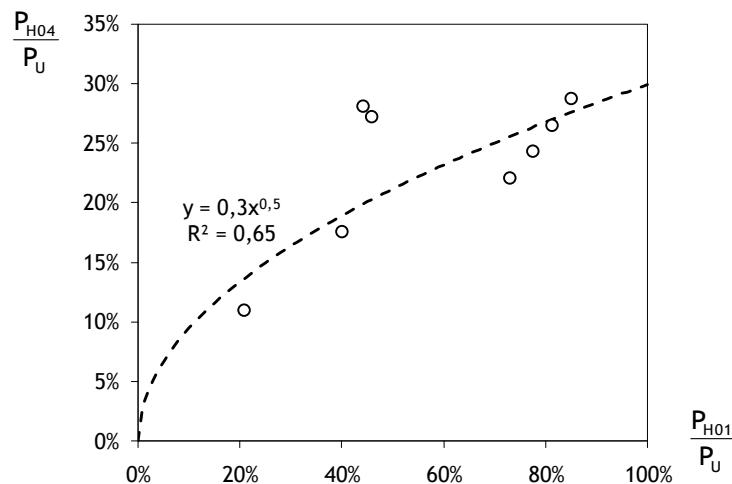
Fig.A7.3 – Ratios between maximum and post-peak experimental pullout loads of hooked fibers.

$$P_{H04} \approx 0.3 \times \sqrt{P_{H01} \times P_U} \qquad\qquad (A7.3)$$

Appendix 8

Application of the engineered expressions on several case-studies

A8.1 INTRODUCTION

In Chapter 8 the formulation of new constitutive model for SFRC was advanced and good agreement with the experimental data reported in Chapter 3 could be attained. Afterwards, engineered expressions for design and optimization (EEDO) were suggested in order to simulate the σ-w curves given by the model through a more straightforward procedure (Section 8.6).

The suitability of the new EEDO on reproducing the new constitutive model was analyzed by calculating the tensile responses of the case-studies defined in Table 8.5. The objective of this appendix is to give additional data for the reader to judge on the applicability of this alternative approach under several different scenarios.

This appendix compares the σ-w curves given by the new constitutive model and by the EEDO for straight and hooked steel fibers. In both cases, the inputs and outputs of the EEDO are summarized and the comparative graphs for the 12 case studies considered are then given.

A8.2   STRAIGHT STEEL FIBERS

Table A8.1 – Values of the parameters defining the EEDO of SFRC with straight fibers.

		CASES												
		0	1	2	3	4	5	6	7	8	9	10	11	12
INPUTS														
d	[mm]	0.75	0.50	1.00	---	---	---	---	---	---	---	---	---	---
L	[mm]	45	---	---	30	60	---	---	---	---	---	---	---	---
f_y	[MPa]	1100	---	---	---	---	600	2100	---	---	---	---	---	---
f_{ck}	[MPa]	30	---	---	---	---	---	---	45	60	---	---	---	---
V_f	[%]	0.38	---	---	---	---	---	---	---	---	0.57	0.76	---	---
η_θ	[-]	0.50	---	---	---	---	---	---	---	---	---	---	0.65	0.80
A_{sec}	[cm^2]	225	---	---	---	---	---	---	---	---	---	---	---	---
P_{S01}	[N]	39.2	26.1	52.2	26.1	52.2	---	---	51.3	58.9	---	---	---	---
P_{S02}	[N]	19.6	13.1	26.1	13.1	26.1	---	---	25.7	29.4	---	---	---	---
w_{S01}	[mm]	0.10	---	---	---	---	---	---	---	---	---	---	---	---
w_{S02}	[mm]	0.20	---	---	---	---	---	---	---	---	---	---	---	---
w_{S03}	[mm]	11.3	---	---	7.5	15.0	---	---	---	---	---	---	---	---
OUTPUTS														
B_C		2.896	2.896	2.896	2.896	2.896	2.896	2.896	2.896	2.896	2.896	2.896	2.896	2.896
k_C		39.764	39.764	39.764	39.764	39.764	39.764	39.764	39.764	39.764	39.764	39.764	39.764	39.764
c_C		1.000	1.000	1.000	1.000	1.000	1.000	1.000	1.000	1.000	1.000	1.000	1.000	1.000
n_C		1.000	1.000	1.000	1.000	1.000	1.000	1.000	1.000	1.000	1.000	1.000	1.000	1.000
B_{ER}		2.102	2.102	2.102	2.102	2.102	1.146	4.013	2.102	2.102	3.153	4.204	2.732	3.363
k_{ER}		3.417	3.417	3.417	3.229	2.839	3.242	3.767	3.417	3.417	3.639	3.861	3.514	3.612
c_{ER}		3.064	3.105	2.700	2.944	2.914	2.714	3.764	3.168	3.271	3.109	3.154	3.314	3.564
n_{ER}		0.503	0.506	0.499	0.506	0.499	0.503	0.503	0.500	0.498	0.503	0.503	0.474	0.444
B_B		2.102	2.102	2.102	2.102	2.102	1.146	4.013	2.102	2.102	3.153	4.204	2.732	3.363
k_B		3.203	3.096	3.256	3.095	2.603	2.930	3.604	3.137	3.096	3.411	3.619	3.229	3.251
c_B		3.399	3.537	2.973	3.363	3.149	3.165	4.033	3.568	3.718	3.447	3.495	3.724	4.059
n_B		0.503	0.506	0.499	0.506	0.499	0.503	0.503	0.500	0.498	0.503	0.503	0.474	0.444

Fig.A8.1 – Predicted σ-w responses of SFRC with straight fibers for cases 1 to 6.
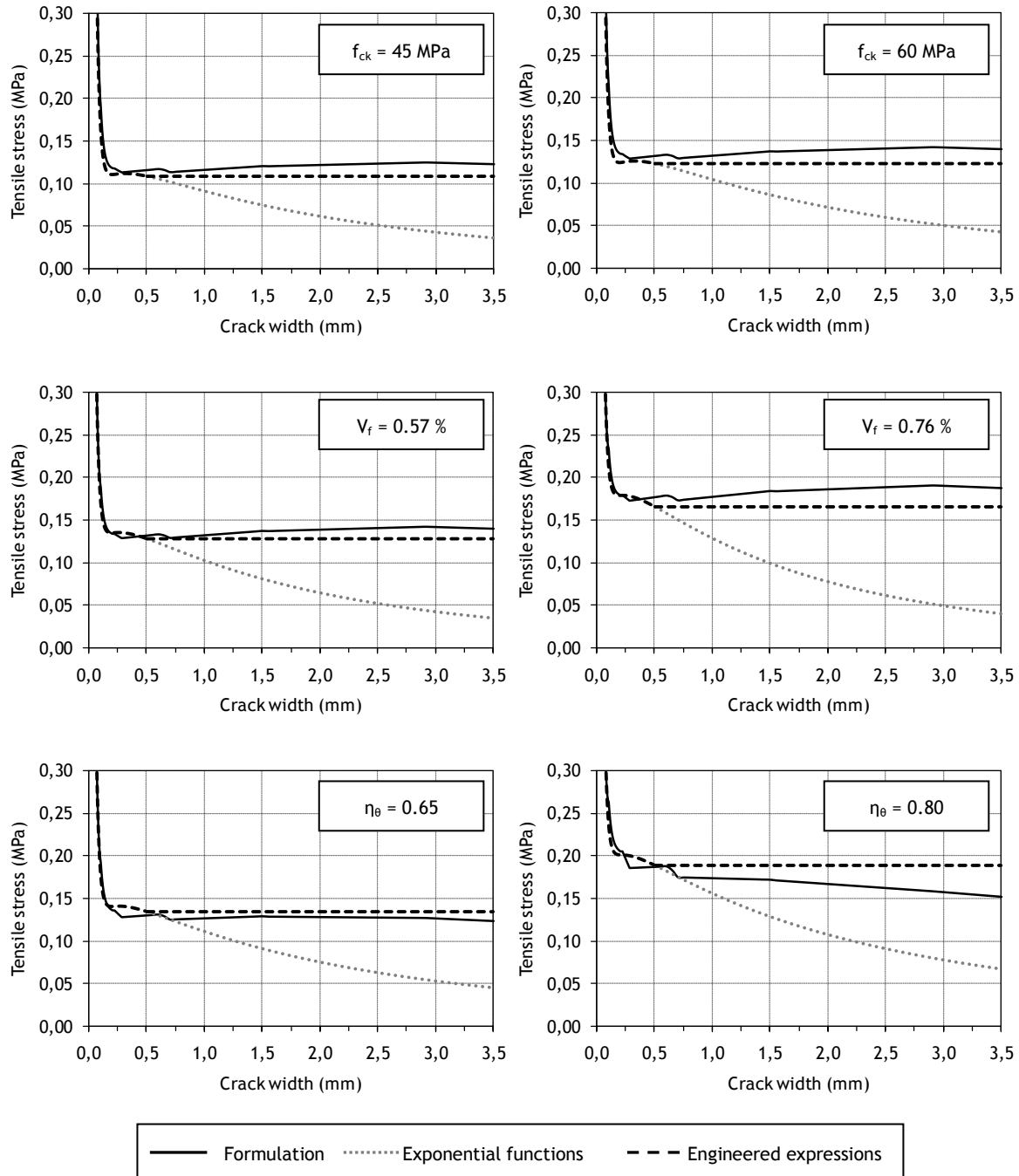
Fig.A8.2 – Predicted σ-w responses of SFRC with straight fibers for cases 7 to 12.

A8.2.3 HOOKED STEEL FIBERS

Table A8.2 – Values of the parameters defining the EEDO of SFRC with hooked fibers.

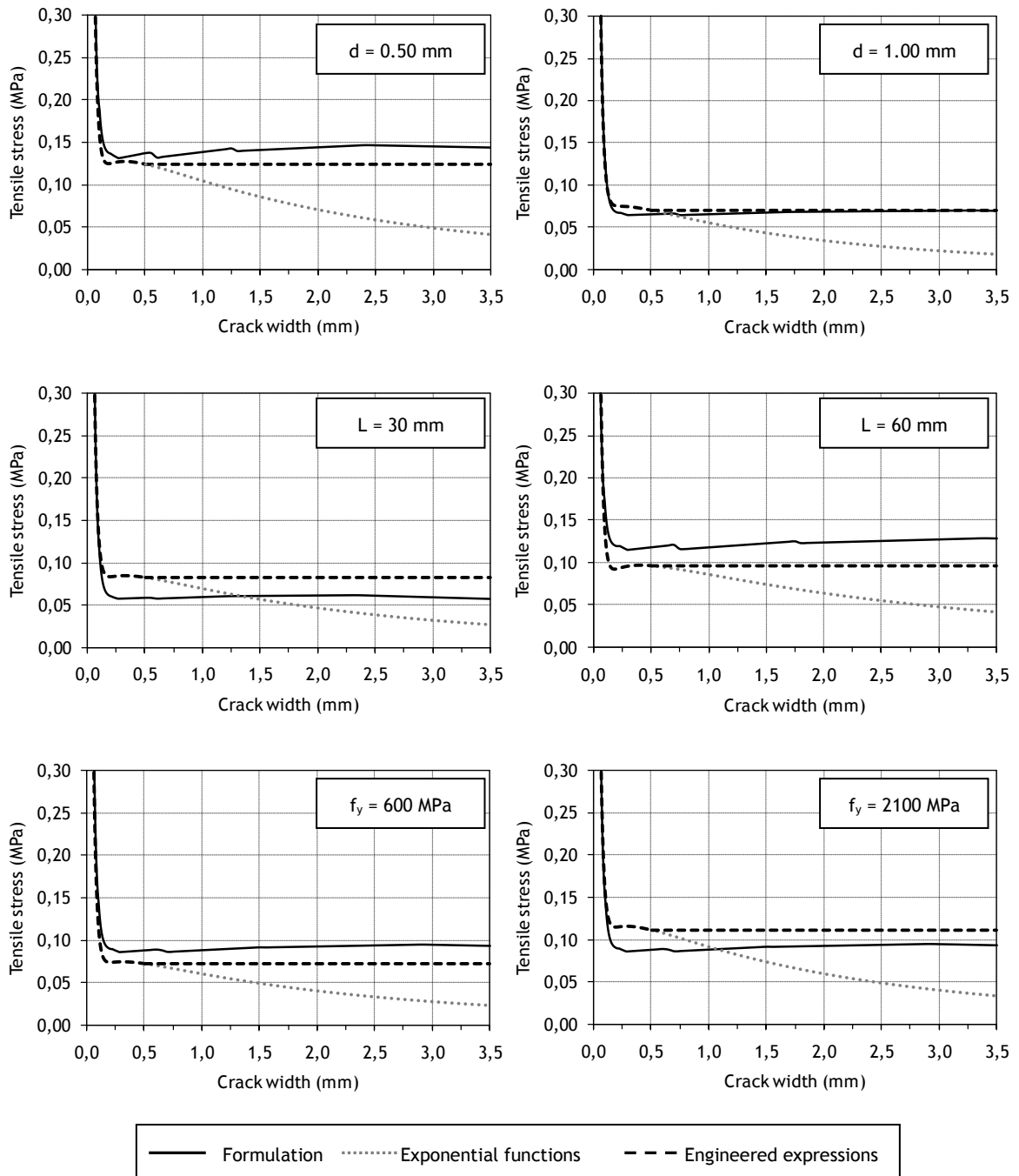|		CASES												
		0	1	2	3	4	5	6	7	8	9	10	11	12
INPUTS														
d	[mm]	0.75	0.50	1.00	---	---	---	---	---	---	---	---	---	---
L	[mm]	45	---	---	30	60	---	---	---	---	---	---	---	---
f_y	[MPa]	1100	---	---	---	---	600	2100	---	---	---	---	---	---
f_{ck}	[MPa]	30	---	---	---	---	---	---	45	60	---	---	---	---
V_f	[%]	0.38	---	---	---	---	---	---	---	---	0.57	0.76	---	---
η_θ	[-]	0.50	---	---	---	---	---	---	---	---	---	---	0.65	0.80
A_{sec}	[cm^2]	225	---	---	---	---	---	---	---	---	---	---	---	---
P_{S01}	[N]	39.2	26.1	52.2	26.1	52.2	---	---	51.3	58.9	---	---	---	---
P_{S02}	[N]	19.6	13.1	26.1	13.1	26.1	---	---	25.7	29.4	---	---	---	---
w_{S01}	[mm]	0.10	---	---	---	---	---	---	---	---	---	---	---	---
w_{S02}	[mm]	0.20	---	---	---	---	---	---	---	---	---	---	---	---
w_{S03}	[mm]	11.3	---	---	7.5	15.0	---	---	---	---	---	---	---	---
P_{H01}	[N]	267.4	118.9	475.5	---	---	---	---	350.4	402.1	---	---	---	---
P_{H04}	[N]	108.2	48.1	192.3	---	---	130.4	149.4	123.8	132.6	---	---	---	---
w_{H01}	[mm]	0.60	---	---	---	---	---	---	---	---	---	---	---	---
w_{H04}	[mm]	4.85	---	---	---	---	---	---	---	---	---	---	---	---
OUTPUTS														
B_C		2.896	2.896	2.896	2.896	2.896	2.896	2.896	2.896	2.896	2.896	2.896	2.896	2.896
k_C		39.764	39.764	39.764	39.764	39.764	39.764	39.764	39.764	39.764	39.764	39.764	39.764	39.764
c_C		1.000	1.000	1.000	1.000	1.000	1.000	1.000	1.000	1.000	1.000	1.000	1.000	1.000
n_C		1.000	1.000	1.000	1.000	1.000	1.000	1.000	1.000	1.000	1.000	1.000	1.000	1.000
B_{ER}		2.102	2.102	2.102	2.102	2.102	1.146	4.013	2.102	2.102	3.153	4.204	2.732	3.363
k_{ER}		3.078	3.078	3.078	3.078	3.078	4.558	1.918	3.228	3.378	3.078	3.078	3.879	4.809
c_{ER}		27.420	21.170	33.670	27.420	27.420	26.320	29.620	18.045	19.920	27.420	27.420	27.608	26.670
n_{ER}		0.617	0.617	0.617	0.654	0.579	0.617	0.617	0.617	0.617	0.617	0.617	0.607	0.598
B_B		2.102	2.102	2.102	2.102	2.102	1.146	4.013	2.102	2.102	3.153	4.204	2.732	3.363
k_B		1.736	1.736	1.736	1.736	1.736	0.129	1.530	1.295	0.892	1.736	1.736	2.020	2.339
c_B		51.233	41.496	60.970	51.223	51.233	83.613	43.515	39.560	45.223	51.233	51.233	52.903	53.044
n_B		0.617	0.617	0.617	0.654	0.579	0.617	0.617	0.617	0.617	0.617	0.617	0.607	0.598
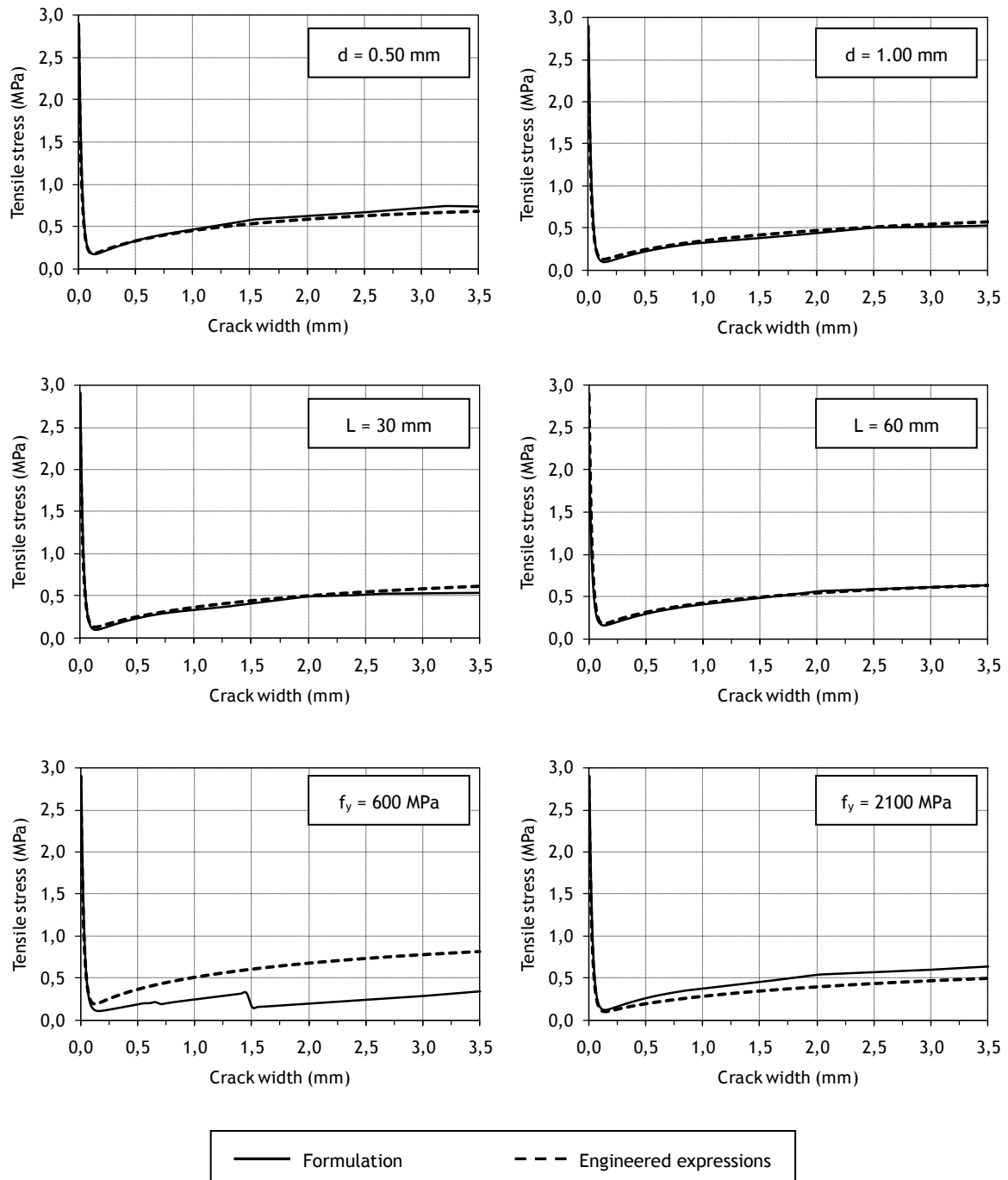
Fig.A8.3 – Predicted σ-w responses of SFRC with hooked fibers for cases 1 to 6.
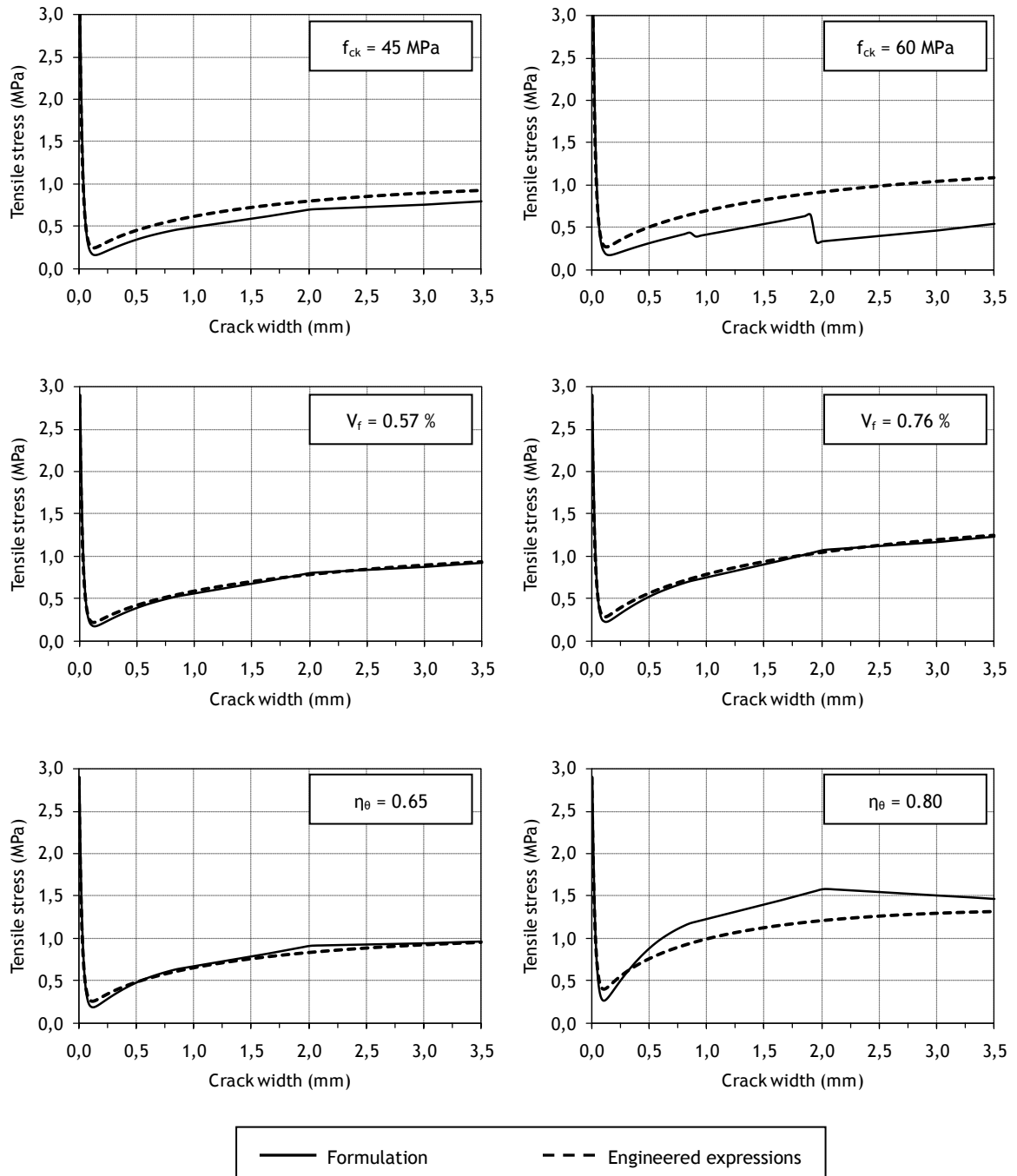
Fig.A8.4 – Predicted σ-w responses of SFRC with hooked fibers for cases 7 to 12.

Notations and symbols

<u>Properties of plain concrete</u>

f_{ck} = Characteristic compressive strength of the cement matrix .... [MPa]

f_{cm} = Average compressive strength of the cement matrix .... [MPa]

f_{ctm} = Average tensile strength of the cement matrix .... [MPa]

E_m = Elastic modulus of the cement matrix .... [MPa]

<u>Properties of steel fibers</u>

L = Fiber length .... [mm]

d = Fiber diameter .... [mm]

A_f = Fiber cross-sectional area .... [mm^2]

E_f = Elastic modulus of the steel fibers .... [MPa]

f_y = Tensile yield strength of steel fibers .... [MPa]

f_u = Ultimate tensile strength of steel fibers .... [MPa]

G_1 = End section of the fiber hooked-end .... [-]

G_2 = Intermediate section of the fiber hooked-end .... [-]

G_3 = Section of the fiber hooked-end close to the straight segment .... [-]

<u>Parameters of the new constitutive model</u>

σ_C = Tensile stress of plain concrete in the cross-section .... [MPa]

σ_{SF} = Tensile stress of steel fibers in the cross-section .... [MPa]

σ_{SFRC} = Tensile stress of SFRC in the cross-section .... [MPa]

V_f = Volume fraction of fibers .... [%]

M_f = Mass fraction of fibers .... [kg/m^3]

N_f = Total number of fibers in the cross-section .... [-]

$N_{\theta i}$ = Number of fibers in the cross-section at inclination angle θ_i .... [-]

$L_{e,max}$ = Maximum fiber embedded length .... [mm]

$L_{e,crit}$ = Critical fiber embedded length .... [mm]

$L_{e,average}$ = Average fiber embedded length .... [mm]

$P_{\theta i}$ = Pullout load at inclination angle θ_i .... [N]

$P_{N,\theta i}$ = Overall pullout load of N fibers at inclination angle θ_i .... [N]

<u>Parameters of the Engineered Expressions for Design and Optimization</u>

σ_{ER} = Tensile stress of the equivalent rebar in the cross-section .... [MPa]

σ_B = Tensile stress of bond between fibers and the matrix in the cross-section .... [MPa]

B_C = Parameter accounting for the maximum tensile stress of plain concrete .... [MPa]

B_{ER} = Parameter accounting for the tensile yield strength of the SFRC cross-section.... [MPa]

B_B = Parameter accounting for the maximum decay of bond strength

between fibers and the matrix in the SFRC cross-section .... [MPa]

k_C = Parameter controlling the accounting for the maximum tensile stress

of plain concrete... [MPa]

Features of fiber pullout tests

P   = Pullout load (orthogonal to cracked surface) .... [N]

δ   = Displacement along load direction .... [mm]

w   = Crack width along load direction .... [mm]

Δw   = Increment of crack width along load direction .... [mm]

L_e = Shorter fiber embedded length within the cement matrix .... [mm]

θ   = Fiber inclination angle relatively to load direction ....[°]

N   = Number of sides of the cracked section at which spalling of the matrix occurs .... [-]

k   = Parameter taking into account the pullout test configuration ....[-]

Parameters of pullout models

μ   = Friction coefficient between steel fibers and the cement matrix ....[-]

$τ_{max}$ = Maximum interfacial shear stress .... [MPa]

$τ_{fric}$ = Friction interfacial shear stress .... [MPa]

$τ^*$ = Apparent interfacial shear stress .... [MPa]

$τ(s)$ = Distribution of interfacial shear stress .... [MPa]

Parameters associated to modeling of the pullout responses of straight fibers

S_i = Key-point *i* governing the shape of the pullout diagram of straight

fibers inclined relatively to the loading direction ....[-]

S_{i0} = Key-point *i* governing the shape of the pullout diagram of straight

fibers aligned relatively to the loading direction ....[-]

P_{Si} = Pullout load at key-point S_i .... [N]

P_{SAi} = Aligned component of the pullout load at key-point S_i .... [N]

P_{SN} = Non-aligned component of the pullout load .... [N]

w_{Si} = Crack width at key-point S_i .... [mm]

w_{SAi} = Aligned component of the crack width at key-point S_i .... [mm]

w_{SNi} = Non-aligned component of the crack width at key-point S_i .... [mm]

$L_{eff(S2)}$ = Effective fiber length factor at point S_2 .... [-]

L_d = Extension of the debonded segments of the fiber .... [mm]

$L_{S,crit}$ = Critical straight fiber embedded length for pullout.................................... [mm]

Parameters associated to modeling of the pullout responses of hooked fibers

H_i = Key-point i governing the shape of the pullout diagram of hooked fibers inclined relatively to the loading direction .... [-]

H_{i0} = Key-point i governing the shape of the pullout diagram of hooked fibers aligned relatively to the loading direction .... [-]

P_{Hi} = Pullout load at key-point H_i .... [N]

P_{HAi} = Component of the pullout load at key-point H_i derived from the direction of the original embedded part of the fiber .... [N]

P_{HN} = Component of the pullout load derived from the direction orthogonal to the original embedded part of the fiber .... [N]

w_{Hi} = Crack width at key-point H_i .... [mm]

w_{HAi} = Component of the crack width at key-point Hi derived from the direction of the original embedded part of the fiber .... [mm]

w_{HNi} = Component of the crack width at key-point H_i derived from the direction orthogonal to the original embedded part of the fiber .... [mm]

Δw_{H0i} = Increment of crack width during the stage *i* of the straightening process of the hook .... [mm]

ΔP_{H0i} = Increment of pullout load during the stage *i* of the straightening process of the hook .... [N]

$L_{eff\ (Hi)}$ = Effective fiber length factor at point H_i .... [-]

$L_{H,crit}$ = Critical hooked fiber embedded length for pullout .... [mm]

Parameters associated to spalling of the matrix

L_{SP1} = Length of spalled matrix generated by P_{S01} .... [mm]

L_{SP2} = Increment of spalled matrix generated by P_{H01} .... [mm]

Δw_{SP1} = Increment of crack width due to matrix spalled length L_{SP1} .... [mm]

Δw_{SP2} = Increment of crack width due to matrix spalled length L_{SP2} .... [mm]

A_{SP1} = Surface failure of the wedge of spalled matrix with length L_{SP1} .... [mm^2]

A_{SP2} = Surface failure of the wedge of spalled matrix with length L_{SP2} .... [mm^2]

D_{F1} = Deviation force at fiber exit point generated by P_{S01} .... [N]

R_{SP1} = Resisting force provided by the matrix wedge against spalling .... [N]

F_{SP1} = Component of D_{F1} which generates matrix spalled length L_{SP1} .... [N]

F_{R1} = Component of D_{F1} parallel to the embedded part of the fiber .... [N]

D_{F2} = Deviation force at fiber exit point generated by P_{H01} .... [N]

F_{SP2} = Component of D_{F2} which generates matrix spalled length L_{SP2} .... [N]

a_1 = Second order term of the quadratic function used to obtain L_{SP1} .... [-]

b_1 = First order term of the quadratic function used to obtain L_{SP1} .... [mm]

c_1 = Constant term of the quadratic function used to obtain L_{SP1} .... [mm^2]

a_2 = Second order term of the quadratic function used to obtain L_{SP2} ....[-]

b_2 = First order term of the quadratic function used to obtain L_{SP2} .... [mm]

c_2 = Constant term of the quadratic function used to obtain L_{SP2} .... [mm^2]

Parameters associated to fiber rupture

$f_{u(\theta)}$ = Ultimate tensile strength of inclined steel fibers at angle θ ....[MPa]

P_u = Average ultimate pullout load of aligned steel fibers .... [N]

$P_{u(\theta)}$ = Average ultimate pullout load of inclined steel fibers at angle θ .... [N]

ε_u = Ultimate strain of the steel fibers .... [‰]

ε_a = Strain of the steel fibers due to axial loading .... [‰]

ε_c = Strain of the steel fibers due to curvature at fiber exit point .... [‰]

$\Delta\varepsilon_p$ = Plastic strain range of the steel fibers constitutive diagram .... [‰]

R_F = Idealized fiber radius of curvature at failure .... [mm]

R_P = Component of R_F due to steel yielding .... [mm]

R_C = Component of R_F due to curvature at fiber exit point .... [mm]

Parameters of fiber orientation

η = Orientation number ....[-]

η_M = η after mixing FRC ....[-]

η_C = η after casting FRC into the formwork ....[-]

η_D = η after occurrence of dynamic effects ....[-]

η_F = η after wall-effects induced by the formwork ....[-]

η_θ = η in the hardened-state ....[-]

η_x = η along the x-axis ....[-]

η_y = η along the y-axis ....[-]

η_z = η along the z-axis ....[-]

η_{xz} = Sum of η in the x-and z-axes ....[-]

η_{xyz} = Sum of η in the x-, y-and z-axes ....[-]

η_{1D} = η in the unidirectional case (1-D) ....[-]

η_{2D} = η in the planar-random case (2-D) ....[-]

η_{3D} = η in the spatial-random case (3-D) ....[-]

η_0 = η at the zone of the cross-section in bulk ....[-]

η_{C0} = η at the zone of the cross-section in bulk after casting ....[-]

η_{D0} = η at the zone of the cross-section in bulk after dynamic effects ....[-]

η_1 = Average η at the zone of the cross-section with one boundary condition ....[-]

η_2 = Average η at the zone of the cross-section with two orthogonal

               boundary conditions ....[-]

$\Delta\eta_{Ci}$ = Increment of η in direction *i* due to casting method ....[-]

$\Delta\eta_{CW}$ = Increment of η due to wall-effects of the casting element .... [-]

CDi = Parameter accounting for misalignment between casting direction

and direction i of the formwork .... [-]

$\Delta\eta_{Di}$ = Increment of η in direction *i* due to dynamic effects .... [-]

$\Delta\eta_{DVi}$ = Increment of η in direction *i* due to external vibration .... [-]

$\Delta\eta_{DFi}$ = Increment of η in direction *i* due to flow .... [-]

$\Delta\eta_{FWi}$ = Increment of η in direction *i* due to wall-effects of the formwork .... [-]

$\eta_{xz,m}$ = Average sum of η_{xz} .... [-]

$\eta_{xyz,m}$ = Average sum of η_{xyz} .... [-]

$\Delta\eta_{W}$ = Increment of η due to wall-effects .... [-]

$\sigma(\eta_{xz})$ = Standard deviation of η_{xz} .... [-]

$\sigma(\eta_{xyz})$ = Standard deviation of η_{xyz} .... [-]

φ = Vertical angle (starting from the plane xOz) .... [°]

β = Horizontal angle (within plane xOz, starting from the x-axis) .... [°]

A_ξ = Spherical surface associated to the angle ξ in half-sphere .... [mm²]

ξ = Angle around an independent axis .... [°]

SL = Significance level .... [-]

ξ_{SL} = Angle around an independent axis providing a significance level α .... [°]

$f(\theta_i)$ = Gaussian frequency of fibers with inclination angles θ_i .... [%]

$p(\theta_i)$ = Frequency of fibers with inclination angles θ_i in the cross-section.................... [%]

Parameters associated to the geometry of the cross-section of the element

D_C = Diameter of concrete in the cross-section of the casting element .... [mm]

B_C = Width of concrete in the cross-section of the casting element .... [mm]

H_C = Height of concrete in the cross-section of the casting element .... [mm]

$H_{C,eff}$ = Effective H_C .... [mm]

h_i = Distance between fiber gravity point and the horizontal boundary condition .... [mm]

b_i = Distance between fiber gravity point and the vertical boundary condition .... [mm]

A_{sec} = Area of the cross-section .... [mm²]

A_0 = Area of the cross-section with zero boundary conditions .... [mm²]

A_1 = Area of the cross-section with one boundary condition .... [mm²]

A_2 = Area of the cross-section with two orthogonal boundary conditions .... [mm²]

Publications related to this research

Journal papers

Laranjeira F, Aguado A, Molins C (2009) Predicting the pullout response of inclined straight steel fibers, Journal of Materials and Structures (available online since November 2009: DOI 10.1617/s11527-009-9553-4).

Laranjeira F, Aguado A, Molins C. Predicting the pullout response of inclined hooked steel fibers (Under revision process at *Cement and Concrete Research*).

Laranjeira F, Grünewald S, Walraven J, Blom C, Molins C, Aguado A. Characterization of the orientation profile in fiber reinforced concrete (to be submitted to *Cement and Concrete Research*).

Laranjeira F, Aguado A, Molins C, Grünewald S, Walraven J, Cavalaro S. Framework to predict the orientation of fibers in FRC: A novel philosophy" (to be submitted to *Engineering Fracture Mechanics*)

Conferences

Laranjeira F, Aguado A, Molins C (2009) Métodos numéricos en la caracterización de hormigones con fibras: una nueva perspectiva, Métodos Numéricos en Ingeniería 2009, June 2009, Barcelona, Spain. Eds.: A. Huerta, Oñate E., Rodríguez Ferran, I.N. Figueiredo, L.F. Menezes, A.J.B. Tadeu. ISBN: 978-84-96736-66-5.

Laranjeira F, Molins, C, Aguado A (2008) Comportamiento a tracción de hormigones reforzados con fibras de acero, Proceedings from the 4th International Structural Concrete Conference (ACHE), November 2008, Valencia, Spain. ISBN: 978-84-89670-62-4. D.L.: M-485-89-2008. pp.283-284 summary and 10 pages full paper in CD-ROM.

Laranjeira F, Aguado A, Molins C (2008) Evaluating uniaxial tensile behavior of steel fiber reinforced concrete using a meso-scale model, Proceedings of the 7th RILEM Symposium on FRC: Design and applications (BEFIB), September 2008, Chennai, India. ISBN: 978-2-35158-064-6. pp.1079-1088.

Laranjeira F, Aguado A, Molins C (2008) *Equação constitutiva de betão reforçado com fibras*, 2[º] Congresso Nacional da Prefabricação em Betão. ANIPB 2008 (Associação Nacional dos Industriais da Prefabricação em Betão). Lisbon, Portugal.

de la Fuente A, Laranjeira F, Molins C, Aguado A (2008) *Aplicações estruturais de betão reforçado com fibras. Modelo de análise estrutural aplicado a tubos de saneamento*, 2^0 Congresso Nacional da Prefabricação em Betão. ANIPB 2008 (Associação Nacional dos Industriais da Prefabricação em Betão). Lisbon, Portugal.

Aguado A, Laranjeira F (2007) Presentación del anejo de hormigón con fibras de la EHE", *Jornada Técnica de aplicaciones estructurales de hormigón con fibras*, Barcelona, 2007, pp.1-32. Cátedra de empresas patrocinada por Basf Molins Bekaert-UPC (www.bmbupc.org)

Laranjeira F, Aguado A, Molins C (2007) Constitutive equations of fiber reinforced concrete, *CD-ROM Proceedings of the ECCOMAS Thematic Conference on Computational Methods in Tunneling (EURO:TUN 2007),* August 27-29, 2007, Vienna, Austria, Eds.: J. Eberhardsteiner, G. Beer, Ch. Hellmich, H.A. Mang, G. Meschke, W. Schubert, Publisher: Vienna University of Technology, Austria, ISBN: 978-3-9501554-7-1